HOKKAIDO UNIVERSITY

Title	Control of dynamic fracturing in concrete pile head breakage by blasting
Author(s)	金, 学晩
Degree Grantor	北海道大学
Degree Name	博士(工学)
Dissertation Number	甲第11579号
Issue Date	2014-09-25
DOI	https://doi.org/10.14943/doctoral.k11579
Doc URL	https://hdl.handle.net/2115/57234
Type	doctoral thesis
File Information	Hak-Man_Kim.pdf

Hokkaido University Collection of Scholarly and Academic Papers : HUSCAP

CONTROL OF DYNAMIC FRACTURING IN CONCRETE PILE HEAD BREAKAGE BY BLASTING

HAKMAN KIM

Graduate School of Engineering
Hokkaido University
2014

CONTROL OF DYNAMIC FRACTURING IN CONCRETE PILE HEAD BREAKAGE BY BLASTING

HAKMAN KIM

Graduate School of Engineering
Hokkaido University
2014

DISSERTATION ABSTRACT

博士の専攻分野の名称： 博士（工学） 氏名：HakMan Kim

Title of dissertation submitted for the degree

（学位論文題目）

Control of dynamic fracturing in concrete pile head breakage by blasting

（発破による杭頭処理における動的破壊の制御）

<Abstract>

Deep foundations generally include as piles, drilled shafts, caissons and piers. In many countries, drilled shafts have been utilized as a foundation of ground structures because these can resist both axial and lateral loads and minimize the settlement of the foundation. However, in the case of cast-in-place concrete piles, a top part of the concrete pile, i.e. concrete pile head, should be adjusted to the bottom level of main foundation and, thus, the breakage of concrete pile head is required. However, the

breakage of concrete using mechanical methods involves with various risks with respect to safety. Therefore, alternative methods to solve the problem are required.

This dissertation investigates a new dynamic fracturing method for the breakage of concrete pile head by blasting. The dissertation consists of six chapters.

In chapter 1, the background and purpose of the dissertation are described and the literature related to dynamic fracturing of rock-like materials by blasting are reviewed. Especially, it is pointed out that knowledge of 3-dimensional fracture process by cylindrical charge is indispensable to consider the optimal blasting condition for the concrete pile head breakage.

In chapters 2 and 3, Dynamic Fracture Process Analysis for axisymmetric problem (DFPA-A) is proposed and the fracture process in a cylindrical body with a cylindrical charge is discussed. In chapter 2, DFPA for 2-dimensional plane strain problem is reviewed and DFPA-A is formulated. In chapter 3, a numerical code of DFPA-A is developed and its applicability is verified. In DFPA-A, two kinds of tensile fracture, i.e., the tensile fractures within *r-z* plane and normal to *r-z* plane in the cylindrical coordinate (r, z, θ), are taken into account. In the modeling of the tensile fracture within *r-z* plane, inter cracking method is used to simulate crack initiation, propagation and coalescence and the cohesive law is adopted to simulate the nonlinear crack opening behavior due to the existence of fracture process zone near the crack tip. In the modeling of the tensile fracture normal to *r-z* plane, the stress-strain relation in each element is used to express the decohesion of crack surface. A concept of Crack

Opening Strain (COS) is proposed for the modeling of cohesive law where COS is defined as the ratio of the Crack Opening Displacement (COD) to arch length of subdomain which includes one predominant crack. Numerical results of fracture process under various conditions are shown and it is clarified that the conical crack pattern was formed from the bottom of charge hole as well as predominant cracks radially extending from the charge hole in the axisymmetric condition. This result indicates that, in the concrete pile breakage, the propagation of conical cracks should be controlled to prevent the damage in the remaining part of the pile. Additionally, the fracture process obtained from axisymmetric condition is compared with that from plane strain condition and the validity of the proposed method as well as the range in which plane strain condition is applicable are discussed.

In chapter 4, for the controlling of the conical cracks from the bottom of charge hole, the laboratory scale experiment and numerical analysis of the dynamic fracturing in cylindrical concrete pile with hollow steel plate as a crack arrester are performed. To prove the effectiveness of hollow steel plate as a crack arrester for the purpose of minimization of the damages in the remaining part of concrete pile, two types of experiments and DFPA-A with/without the application of the steel plate are conducted and the applicability of the steel plate is shown. Then, assuming the laboratory-scale experiment of concrete pile head removal by blasting a cylindrical charge with a hollow steel plate, DFPA-A is conducted to investigate the influence of both the loading rate

and spacing between steel plate and charge hole on the resultant fracture pattern, and the obtained fracture patterns are compared.

In chapter 5, for the controlling of the crack propagation direction by the use of wedged charge holder, DFPA for 2-dimensional plane strain condition is performed and the influence of loading conditions on the resultant fracture patterns are investigated. By analyzing numerical results, the optimal pressure function to obtain smoother fracture plane and to minimize damage in the remaining part is clarified. Furthermore, the relation between the crack velocity and crack branching is discussed.

In chapter 6, the obtained results are reviewed and some suggestions for future work are given.

TABLE OF CONTENTS

ABSTRACT ····· ii

1. INTRODUCTION

1.1 BACKGROUND ····· 1

1.2 LITERATURE REVIEW AND PROSPECTS ····· 3

1.2.1 Rock and concrete breakage by blasting ····· 3

1.2.2 Dynamic fracture of rock-like material ····· 4

1.3 OBJECTIVE OF THIS DISSERTATION ····· 6

1.4 SYNOPSIS OF THIS DISSERTATION ····· 6

BIBLIOGRAPHY ····· 8

2. PROPOSAL OF DYNAMIC FRACTURE PROCESS ANALYSIS FOR AXISYMMETRIC PROBLEM

2.1 INTRODUCTION ····· 13

2.2 DFPA FOR TWO-DIMENSIONAL PLANE PROBLEM ····· 14

2.2.1 Finite Element Formulation ····· 14

2.2.2 Modeling of Tensile fracture ····· 16

2.2.3 Modeling of Strength distribution ····· 17

2.3 DFPA FOR AXISYMMETRIC PROBLEM (DFPA-A) ····· 18

2.3.1 Finite Element Formulation ····· 18

2.3.2 Modeling of Tensile fracture ····· 20

2.3.3 Modeling of Strength distribution ····· 24

2.4 CONCLUDING REMARKS ····· 25

BIBLIOGRAPHY ····· 27

3. APPLICATION OF DYNAMIC FRACTURE PROCESS ANALYSIS FOR AXISYMMETRIC PROBLEM

3.1 INTRODUCTION ····· 30

3.2 MODEL DESCIPTION ····· 31

3.3 NUMERICAL RESULTS ····· 34

3.3.1 Fracture process in rock-like material with a cylindrical charge hole ····· 34
3.3.2 Influence of the bottom shape of charge hole ····· 34
3.3.3 Influence of heterogeneity ····· 38
3.4 DISCUSSION ····· 39
3.5 CONCLUDING REMARKS ····· 41
BIBLIOGRAPHY ····· 43

4. FRACTURE CONTROL IN CYLINDRICAL CONCRETE PILE BY STEEL PLATE
4.1 INTRODUCTION ····· 45
4.2 EXPERIMENTAL ····· 45
4.2.1 Experiment setup ····· 46
4.2.2 Experimental results ····· 47
4.3 NUMERICAL SIMULATION ····· 49
4.3.1 Model description ····· 49
4.3.2 Fracture pattern in the case with/without steel plate ····· 53
4.4 DISCUSSION ····· 57
4.4.1 Influence of applied pressure on fracture pattern ····· 57
4.4.2 Influence of Spacing between steel plate and charge hole on fracture pattern ···· 58
4.5 CONCLUDING REMARKS ····· 60
BIBLIOGRAPHY ····· 62

5. FRACTURE CONTROL IN CONCRETE PILE BY CHARGE HOLDER
5.1 INTRODUCTION ····· 64
5.2 EXPERIMENT USING WEDGED CHARGE HOLDER ····· 65
5.2.1 Experimental setup ····· 65
5.3 NUMERICAL RESULTS ····· 67
5.3.1 Model description ····· 67
5.3.2 DFPA Results ····· 70
5.3.3 Comparison of resultant fracture patterns under various loading conditions ····· 74
5.4 DISCUSSION ····· 75
5.5 CONCLUDING REMARKS ····· 79
BIBLIOGRAPHY ····· 80
6. CONCLUSION ····· 82

CHAPTER 1

INTRODUCTION

1.1 BACKGROUND

Deep foundations generally include piles, drilled shafts, caissons and piers. In many countries, drilled shafts have been utilized as a foundation of ground structures such as apartments, skyscrapers and bridges (Won *et al*., 2002) because these can resist both axial and lateral loads and minimize the settlement of the foundation. However, in the case of cast-in-place concrete piles, the top part of the concrete pile, i.e. concrete pile head, should be adjusted to the bottom level of main foundation. In addition, the strength decreasing of the pile head occurs because of laitance[i]. Thus, the breakage of concrete pile head is required. In Fig.1.1, the pile head treatment is shown in time-sequential manner. The treatment consists of (a) leveling the pile head, (b) grinding, (c) crushing the top of the pile, (d) crushing the bottom of the pile, and (e) cutting and stretching the steel wire. However, the breakage of concrete pile head by the conventional mechanical methods involves with various risks with respect to safety not only for site workers but also for general public living in the vicinity, mainly due to noise hazard. Therefore, alternative methods to solve the problem have been required (Takahashi *et al*., 2006). Nakamura *et al*. (2009) suggested a new alternative method, i.e. a dynamic breakage system for concrete pile head utilizing a charge holder and steel plate for controlling crack propagation to

[i]Laitance : A layer of weak and nondurable material containing cement and fines aggregates, brought by bleeding to the top of overwet concrete, the amount of which is generally increased by overworking or overmanipulating concrete at the surface, by improper finishing or by job traffic (Cement and concrete terminology, 1967).

prevent the damage occurring at remaining part of concrete pile by blasting. In the remaining part of concrete pile, conical cracks from bottom of charge hole, i.e. damages on a lower part of concrete pile, occurred in laboratory-scale experiment. Thus, investigation of the achievement of optimal blasting to minimize the damages on a lower part of concrete pile is indispensable.

Tasks		Equipment and tools
Leveling		Leveler, Pen
Grinding		Grinder
Crushing the top of the pile head		Backhoe/ Crusher
Crushing the bottom of the pile head		Hammer
Cutting and stretching the steel wire		Cutter/ Steel rod

Figure 1.1 Conventional concrete pile head treatment (After Kim *et al*., 2009)

This dissertation investigates the aforementioned dynamic fracturing method proposed by Nakamura *et al*. (2009, 2010) for the breakage of concrete pile head by blasting. For that purpose, the methods of analysis that can simulate the fracture process and find an optimal

condition to minimize the damages due to blast in the remaining parts of concrete pile is proposed. The mechanisms of dynamic fracture in the breakage of concrete pile head by blasting are clarified using this method of analysis.

1.2 LITERATION REVIER AND PROSPECTS

1.2.1 Rock and concrete breakage by blasting

The mechanisms of dynamic fracture caused by rock-like materials have been the subject of study in the application to designing mining excavations, civil engineering structures, recovering oil from oil shale, and other fields (*e.g*., Schmidt, 1981; Haghighi *et al*., 1988; Fourney, 1993). In rock breakage, the stress waves make significant contributions to rock fracture. The importance of stress waves in fracturing has been discussed for the last 50 years, and in that time many publications have offered evidence that stress waves are responsible for the breakage and the theories for the contribution of stress waves to rock fragmentation were generalized (Duvall, 1950; Hino, 1956; Duvall and Atchison, 1957; Rinehardt, 1965; Ito and Sassa, 1968). For example, Duvall (1950) proposed the application of strain gauges grouted into rock and determined the characteristics of strain pulse created by dynamite under production conditions. . The stress wave theories, as formulated by Duvall and Atchison (1957), relied on the spall effect created by the reflection of the stress wave from the free face. Later modifications of the theory acknowledge the contribution of the reflected wave in modifying the tangential tensile stress induced by the incident stress wave within the range related to the breakage caused by blasting. The magnitude of the stresses at the interaction between the free face and the burden was about twice the magnitude of the incident tensile stress (Sassa and Ito, 1963). More recent approaches to quantifying the role of stress waves in rock fragmentation have generally used a computation approach (*e.g*., Adams *et al*., 1983; Preece *et al*., 1994; Mortazavi and Katsabanis, 1998).

In order to control crack propagation and minimize damages in rock-like materials due to blast-induced loads. Fourney *et al.* (1978) investigated a controlled blast method to achieve the fracture propagation control by utilizing a ligamented split tube for charge containment. Mohanty (1990) suggested a fracture plane control technique using satellite holes on either side of the central pressurized hole. Mukugi et al. (1992) developed a drilling system with gloving tools making the notched hole in single pass, which is applicable to hard rocks. Nakamura (1999) developed a new breakage system with a charge holder having two wedges to generate cracks along the desired directions in which shock waves due to the detonation of explosives are concentrated at the wedges and directions of crack initiation are controlled well. Then, Nakamura *et al.* (2009) performed blast experiments with a charge holder for laboratory-scale concrete block to investigate the effect of angle of the charge holder. It was found that the angle of the charge holder of 30 degrees was optimal for breakage of concrete block. Base on the this result, several researchers (*e.g.*, Nakamura *et al.* 2010; Kato *et al*. 2009; Nakamura *et al*. 2013) carried out blast experiments for the control of crack propagation in the breakage of a concrete pile head by blasting with a charge holder and steel plate inside concrete pile. Although these experimental results were successful for breakage of concrete pile head, it was difficult to understand the mechanism of crack growth inside the concrete pile.

1.2.2 Dynamic fracture of rock-like material

Dynamic fracture in rock-like materials is affected by the distribution of inherent flaws and the condition of loading rate (*e.g.*, Grady and Kipp, 1987; Whittaker *et al*., 1992). The fracture stresses induced by a high strain rate load can be much higher than those under the same maximum load applied quasi-statically (*e.g*., Ward and Hadley 1993; Leon and Deierlein, 1996; Sherman and Brandon 1998; Abdennadher 2003). Several researchers (*e.g*., Sheckey *et al.*, 1974; Schmidt e*t al*., 1979; Warpinski *et al*., 1979) indicated that dynamic fracture depend on

the stress loading rate, i.e. when the pressure loading rate is too fast, extreme crushing zone of the rock-like materials occurs near the borehole with little or no fracturing.

Grady and Kipp (1987) proposed a continuum mechanics based approach and applied a damage model to study the strain rate dependency of dynamic fracturing. Following this study, various analytical models to predict fractures under dynamic loading conditions were investigated (*e.g*., Preece *et al*., 1994; Liu and Katsabanis, 1997; Miller *et al*., 1999). Even though these studies gave good estimates of fragment size under different strain rates, characterization of crack growth related to stress distribution was difficult.

Recently, numerical methods have been increasingly applied in analyzing fracturing, including extensive use of finite-element-method (FEM)-based simulations. These methods include the FEM featuring the element deletion method (*e.g*., Bandari, 1979), the FEM featuring the interelement crack method (*e.g*., Xu and Needleman 1994; Camacho and Ortiz 1996; Carol *et al*. 1997; Ortiz and Pandolfi 1999; Ruiz *et al*. 2000; Gálvez *et al*. 2002; Segura and Carol 2010) and the extended FEM (*e.g*., Belytschko and Black 1999; Moës *et al*. 1999; Belytschko *et al*. 2001; Stolarska *et al*. 2001; Song and Belytschko 2009). It has been reported that the latter 2 methods perform reasonably with a careful selection of meth size and fracture energy (Song *et al*, 2008). On this basis, many researchers carried out dynamic fracture process analysis (DFPA) code base on the 2-dimensional FEM featuring the interelement crack method (Kaneko 2004; Yamamoto *et al*. 1999; Cho 2003; Cho *et al*. 2003a,b; Cho and Kaneko; Cho *et al*. 2006, 2008. Fukuda *et al*. 2013). DFPA simulates crack initiations, crack growth and crack coalescence. The code considers the rock fracture process, considering the fracture process zone (FPZ), material heterogeneity and size of effect of the strength of material. However, these researchers could not consider fracturing process in rock by blasting with a cylindrical charge because the DFPAs were conducted under plane-strain condition.

1.3 OBJECTIVE OF THIS DISSERTATION

As described above, in experiments proposed by Nakamura et al. (2009, 2010), there could not find the optimal blasting conditions. Therefore, this dissertation investigates the dynamic fracturing method proposed for the breakage of concrete pile head by blasting with a charge holder and steel plate as a crack arrester for the controlling of the conical cracks from the bottom of charge hole. To treat this problem, DFPA for axisymmetric problem (DFPA-A) is proposed. By using this method, the influence of various loading conditions and various installation locations of steel plate on the dynamic fracture process and resultant fracture pattern is investigated. In addition, because rectangular concrete structures cannot be analyzed by DFPA-A, DFPA for 2-dimensional plane strain problem is applied instead in this class of problems. In summary, this dissertation proposes the DFPA-A which can simulate the fracture process and finds an optimal condition to prevent damages in the remaining part of concrete pile due to blast-induced loads.

1.4 SYNOPSIS OF THIS DISSERTATION

This dissertation is divided into six chapters:

Chapter 1. the background and purpose of the dissertation are described and the literature related to dynamic fracturing of rock-like materials by blasting are reviewed. Especially, it is pointed out that knowledge of 3-dimensional fracture process by cylindrical charge is indispensable to consider the optimal blasting condition for the concrete pile head breakage.

Chapter 2. DFPA for 2-dimensional plane strain problem is reviewed and DFPA-A is formulated.

Chapter 3. a numerical code of DFPA-A is developed and its applicability is verified. In

DFPA-A, two kinds of tensile fracture, i.e., the tensile fractures within *r*-*z* plane and normal to *r*-*z* plane in the cylindrical coordinate (*r*, *z*, θ), are taken into account. In the modeling of the tensile fracture within *r*-*z* plane, inter cracking method is used to simulate crack initiation, propagation and coalescence and the cohesive law is adopted to simulate the nonlinear crack opening behavior due to the existence of fracture process zone near the crack tip. In the modeling of the tensile fracture normal to *r*-θ plane, the stress-strain relation in each element is used to express the decohesion of crack surface. A concept of Crack Opening Strain (COS) is proposed for the modeling of cohesive law where COS is defined as the ratio of the Crack Opening Displacement (COD) to arch length of subdomain which includes one predominant crack. Numerical results of fracture process under various conditions are shown and it is clarified that the conical crack pattern was formed from the bottom of charge hole as well as predominant cracks radially extending from the charge hole in the axisymmetric condition. This result indicates that, in the concrete pile breakage, the propagation of conical cracks should be controlled to prevent the damage in the remaining part of the pile. Additionally, the fracture process obtained from axisymmetric condition is compared with that from plane strain condition and the validity of the proposed method as well as the range in which plane strain condition is applicable are discussed.

Chapter 4. for the controlling of the conical cracks from the bottom of charge hole, the laboratory-scale experiment and numerical analysis of the dynamic fracturing in cylindrical concrete pile with steel plate as a crack arrester are performed. The influences of applied loading conditions and spacing between the bottom of the charge hole and steel plate on the fracture process of concrete pile are investigated and the optimal condition to prevent the damages on remaining part of concrete pile are clarified.

Chapter 5. for the controlling of the crack propagation direction by the use of wedged charge holder, DFPA for 2-dimensional plane strain condition is performed and the influence of loading conditions on the resultant fracture patterns are investigated. By analyzing numerical results, the optimal pressure function to obtain smoother fracture plane and to minimize damage in the remaining part is clarified. Furthermore, the relation between the crack velocity and crack branching is discussed.

Chapter 6. the obtained results are reviewed and some suggestions for future work are given.

BIBLIOGRAPHY

1) Abdennadher, A., Zhao, H. and Othman, R., 2003, A study of cellular materials under impact loading. J. Phys. IV. France, Vol.110, pp.441–446.
2) Cement and concrete terminology: a glossary of terms in the field of cement and concrete technology prepared as part of the work of Committee 116, 1967, American Concrete Institute, ACI publication, SP-19
3) Bandari, S., 1979, On the role of stress waves and quasi-static gas pressure in rock fragmentation by blasting, Acta Astronautica 6: 365-383.
4) Belytschko, T. and Black, T., 1999, Elastic crack growth in finite elements with minimal remeshing, Int. J. Numer. Meth. Eng., Vol.45, No.5,pp.601-620.
5) Belytschko, T., Moës, N., Usui, S. and Parimi, C., 2001, Arvitrary discontinuities in finite elements, Int. J. Numer. Meth. Eng., Vol.50, No.4, pp.993-1013.
6) Camacho, G.T. and Ortiz, M., 1996, Computational modeling of impact damage in brittle materials, Int. J. Solids. Struct., Vol.33, pp. 2988-2938.
7) Carol, I., Prat, P.C., and Lopez, C.M., 1997, Normal/share cracking model: Application to discrete crack analysis, J. Eng. Mech., Vol. 123, No. 8, pp. 765-773.
8) Cho, S.H., 2003, Dynamic fracture process analysis of rock and its application to fragmentation control in blasting, Hokkaido University, Dissertation.
9) Cho, S.H., Ogata, Y. and Kaneko, K., 2003a, Strain rate dependency of the dynamic tensile strength of rock. Int. J. Rock. Mech. Min. Sci., Vol.40, No.5, pp. 763-777.
10) Cho, S.H., Nishi, M., Yamamoto, M. and Kaneko, K., 2003b, Fragment size distribution in blasting, Mater. Trans, Vol.44, No.5, pp.951-956.
11) Cho, S.H., Mohanty. B., Ito, M., Nakamiya, Y., Owada, S., Kubota, S., Ogata, Y., Tsubayama, A., Yokota, M. and Kaneko, K., 2006, Dynamic fragmentation of rock by high-voltage pulses, In: Proceedings of 41st US symposium on rock mechanics, Curran Associates, Inc., 06-1118

12) Cho, S.H., Nakamura, Y., Mohanty. B, Yang. H.S, Kaneko. K, 2008, Numerical study of fracture plane control in laboratory-scale blasting, Engineering Fracture mechanics, Vol. 75(13), pp.3966-3984.

13) Cho, S.H. and Kaneko, K., 2004, Influence of the applied pressure wave form on the dynamic fracture processes in rock, Int. J. Rock Mech.Min. Sci., 41:771-784

14) Dally, J.W., Fourney, W.L., and Holloway, D.C., 1975, Influence of containment of the bore hole pressure on explosive-induced fracture, Int. J. Rock Mech. Min. Sci. & Geomech. Abstr. 12: 5-12.

15) Duvall, W.I., 1953, Strain-wave shapes in rock near explosions, Geophysics 18(2): 310-323.

16) Duvall, W.I., and Atchison, T.C., 1957, Rock breakage by explosives. U.S. Bu. Min. R.I. pp. 6679.

17) Fourney, W.L. 1993, Mechanisms of rock fragmentation by blasting. In, Comprehensive Rock Engineering, Principles, Practice and Projects, J. A. Hudson (ed.), Oxford, Pergamon Press, pp. 39-69.

18) Fourney. W.L., Dally. J.W. and Holloway, D.C., 1978, Controlled blasting with ligamented charge holders, Int. J. Rock Mech. Min.Sci. & Geomech. Abstr. Vol. 15, pp.121~129.

19) Fukuda, D., Moriya, K., Kaneko, K., Sasaki, K., Sakamoto. R, Hidani. K, 2012, Numerical simulation of the fracture process in concrete resulting from deflagration phenomena, Int. J. Fract, Vol. 180(2), pp. 163-175

20) Gálvez, J.C., Cervenka, J., Cendón, D.A. and Saoumad, V., 2002, A discrete crack approach to normal/share cracking of concrete, Cem. Concr. Res., Vol. 32, 1567-1585.

21) Grady, D.E., and Kipp, M.E., 1987, Dynamic rock fragmentation. Fracture Mechanics of Rock (Atkinson, B.K., ED.), Academic Press, London, pp. 429-475.

22) Haghighi, R., Britton, R.R., and Skidmore, D., 1988, Modelling gas pressure effects on explosive rock breakage. Int. J. Mining and Geological Eng. Vol.6, pp. 73-79.

23) Hino, K., 1956, Fragmentation of rock through blasting and shock wave theory of blasting, Quart. Colo. Sch. Min. Vol. 51, pp. 191-209.

24) Ito, I., and Sassa, K., 1968, On the mechanism of breakage by smooth blasting, J. of the Mining and Metallurgical Institute of Japan, Vol.84, pp. 1059-1065 [in Japanese].

25) Leon, R.T., Deierlein, G.G., 1996, Considerations for the use quasi-static testing, Earthquake Spectra, Vo.12, No.1, pp. 87–109

26) Liu, Q., and Katsabanis, P.D., 1993, A theoretical approach to the stress waves around a borehole and their effect on rock crushing, Proc. 4st Int. Symp. Rock Fragmentation by Blasting, Balkema, Rotterdam, pp. 9-16.

27) Kaneko, K., Matsunaga, Y., and Yamamoto, M., 1995. Fracture mechanics analysis of fragmentation process in rock blasting. J. Japan Exp. Soc. Vol.58, No.3, pp. 91-99 [in Japanese].

28) Kato, M., Nakamura, Y., Ogata, Y., Kubota, S., Matsuzawa, T., Nakamura, S., Adachi, T., Yamaura, I., Yamamoto, M., 2009, Research on the dynamic fragment control of pile head using a charge holder, Japan Explosive Society, Vol 70 pp. 108-111.

29) Kim, Y.S., Lee, J.B., Kim, S.K., Lee, J.H., 2009, Development of an automated machine for PHC pile head grinding and crushing work, Automation in Construction, Vol. 18, No.6, pp. 737-750.

30) Miller, O., Freund, L.B., and Needleman, A., 1999, Modeling and simulation of dynamic fragmentation in brittle materials, Int. J. Fracture, Vol. 96, pp. 101-125.

31) Moës, N., Dolbow, J. and Belytschko, T., 1999, A finite element method for crack growth without remeshing, Int. J. Numer. Meth. Eng., Vol.46, pp.131-150.

32) Munjiza, A., 1992, Discrete elements in transient dynamics of fractured media. Ph.D. Thesis, University of Wales, University College of Swansea, Wales, UK

33) Nakamura, Y., 1999, Model experiments on effectiveness of fracture plane control methods in blasting. Int. J Blast Fragment. Vol 3, pp. 59-78.

34) Nakamura, Y., Kato, M., Ogata, Y., Okina. Y, Nakamura. S, Yamamoto. M, 2009, Model experiments on fracture plane control in blasting, Japan Explosive Society, pp. 9-120 [In Japanese].

35) Nakamura, Y., Kato, M., Ogata, Y., Yamaura, I., Nakamura, S. and Cho, S.H., 2010, Dynamic fragmentation method using simple-type charge holder for fracture control in blasting, 10th conference on Japan Society of civil engineers, pp.117-120 [In Japanese].

36) Nakamura, S., Takeuchi, H., Nakamura, Y., Higuchi, T., 2013, Development of the dynamic removal method for concrete pile head using charge holder producing horizontal fracture plane, the 7th international conference on explosives and blasting in China, pp. 197-208.

37) Otiz, M. and Pandolfi, A., 1999, Finite-deformation irreversible cohesive elements for three-dimensional crack-propagation analysis, Int. J. Numer. Meth. Eng., Vol. 44, pp. 1267-1282.

38) Preece, D.S., Thorne, B.J., Baer, M.R., and Swegle, J.W., 1994, Computer simulation of rock blasting, a summary of work from 1987 through 1993. Sandia National Laboratories Report, pp.92-1027.

39) Rinehardt, J.S., 1965, Dynamic fracture strength of rocks. Proc. 7th Symposium of Rock Mech., Univ. Park, Penn., pp. 205-208.

40) Ruiz, G., Ortiz, M. and Pandolfi, A., 2000, Three-dimensional finite element simulation of the dynamic Brazilian tests on concrete cylinders, Int. J. Numer. Meth. Eng., Col 48, pp. 963-994.

41) Schmidt, R.A., Boade, R.R., and Bass, R.C., 1979, A new perspective on well shooting-The behavior of contained explosion and deflagrations, 54th Annual Conference SPE of AIME, Las Vegas, Nevada, September.

42) Schmidt, R.A., Warpinski, N.R., Finely, S.J., and Shear, R.C., 1981, Report, SAND81-1239, Sandia National Laboratories, Albuquerque, New Mexico.

43) Segura, J.M., and Carol, I., 2010, Numerical modeling of pressurized fracture evolution in concrete using zero-thickness inetface elements, Eng. Fract. Mech., Vol.77, pp.1386-1399

44) Sheckey, D.A., Curran, D.R., Seama, L., Rosenberg, J.T., and Petersen, C.F., 1974, Fragmentation of rock under dynamic loads, Int. J. Rock Mech. Min. Sci. & Geomech. Abstr. 11: 303-317.

45) Song, J.H. Wang, H. and Belytschko, T., 2008, A comparative study on finite element methods for dynamic fracture, Comput. Mech. Vol.42, pp.239-250.

46) Song, J.H. and Belytschko, T., 2009, Cracking node method for dynamic fracture with finite elements, Int. J. Numer. Meth. Eng., Vol.77, pp.360-385.

47) Stolarska, M., Chopp, D.L., Moës, N. and Belytschko, T., 2001, Modeling crack growth by level sets in the extended finite element method, Int. J. Numer. Meth. Eng., Vol.51, pp.943-960.

48) Takatoshi, I., Masanori. M., Mitsuru. S., 2006, Development of removed pile method with cutting, Preceedings of the world tunnel congress and 32nd ITA Aseembly, pp.22-27.

49) Ward, I.M., Hadley D.W., 1993, An Introduction to the Mechanical Properties of Solid PolymersWiley, Chichester

50) Warpinski N.R., Schmidt R.A., Cooper, P.M., Walling, H.C., and Northrop, D.A., 1979, High energy gas fract: Multiple fracturing in a well bore, 20th U.S. Symp. Rock Mech., Austin, Texas.

51) Won, Y.H., Lee, J.H., Kim, Y.S., Park, S.J., 2002, A Study on the Automation of Pretensioned Spun High Strength Concrete Pile Cutting Work, Architectural Institute of Korea, Vol.18, pp.181-190.

52) Xu, X.P. and Needlman, A., 1994, Numerical simulation of fast crack growth in brittle solids, J. Mech. Phys. Solids., Vol.42, pp.1397-1434.

53) Yamamoto, M., Ichijo, T., Inaba, T., Morooka, K., and Kaneko, K., 1999, Experimental and theoretical study on smooth blasting with electronic delay detonators, Int. J. of Rock Fragmentation by Blasting, Vol.3, No.1, pp.3-24.

CHAPTER 2

PROPOSAL OF DYNAMIC FRACTURE PROCESS ANALYSIS FOR AXISYMMETRIC PROBLEM

2.1 INTRODUCTION

The DFPA for 2-D plane strain problem has been widely adopted to investigate the dynamic fracturing process in various blasting experiments and its applicability has been verified through many researches (e.g., Kaneko *et al*. 1995; Yamamoto *et al*. 1999; Cho 2003; Cho *et al*. 2003a,b; Cho and Kaneko 2004; Cho *et al*. 2006, 2008; Fukuda *et al*. 2013). In addition, the DFPA for 2-D plane strain problem can also be applied to the simulation of a blasting experiment for breakage of rectangular shaped concrete pile head investigated in Chapter 5. However, it is not possible to apply the DFPA for 2-D plane strain problem for the simulation of breakage of concrete pile head by blasting with a charge holder and steel plate as a crack arrester in which the 3-dimentional crack propagation from the bottom part of cylindrical charge hole and crack arrest around steel plate in blasting experiment for breakage of cylindrical concrete pile head should be analyzed. In case of utilizing detonation or deflagration of explosives for fragmentation of rock-like materials, cylindrical charge is generally applied and corresponding geometrical representation of the problem can be considered as axisymmetric (Sassa and Ito, 1972). Therefore, 3-D fracturing process envisioned here can be treated in the context of axisymmetric problem.

In this chapter, DFPA for 2-D plane strain problem will be reviewed and DFPA-A are proposed.

2.2 DFPA FOR 2-D PLANE STRAIN PROBLEM

In this section, the DFPA for 2-D plane strain problem proposed by Cho and Kaneko (2004) is briefly introduced. For details, refer to Cho (2003).

2.2.1 Finite Element Formulation

The basic equations in two-dimensional problems are given by following equations.
The equation of motion:

$$\begin{aligned} \frac{\partial \sigma_{xx}}{\partial x} + \frac{\partial \sigma_{yx}}{\partial y} &= \rho \frac{\partial^2 u_x}{\partial t^2} \\ \frac{\partial \sigma_{xy}}{\partial x} + \frac{\partial \sigma_{yy}}{\partial y} &= \rho \frac{\partial^2 u_y}{\partial t^2} \end{aligned} \tag{2.1}$$

The constitutive equation (visco-elastic stress-strain relation) under plane strain condition:

$$\begin{Bmatrix} \sigma_{xx} \\ \sigma_{yy} \\ \sigma_{xy} \end{Bmatrix} = \frac{E}{(1+\nu)(1-2\nu)} \begin{bmatrix} 1-\nu & \nu & 0 \\ \nu & 1-\nu & 0 \\ 0 & 0 & (1-2\nu)/2 \end{bmatrix} \begin{Bmatrix} \varepsilon_{xx} + \eta \partial \varepsilon_{xx}/\partial t \\ \varepsilon_{yy} + \eta \partial \varepsilon_{yy}/\partial t \\ \gamma_{xy} + \eta \partial \gamma_{xy}/\partial t \end{Bmatrix} \tag{2.2}$$

The strain-displacement relation:

$$\begin{Bmatrix} \varepsilon_{xx} \\ \varepsilon_{yy} \\ \gamma_{xy} \end{Bmatrix} = \begin{Bmatrix} \partial u_x / \partial x \\ \partial u_y / \partial y \\ \partial u_y / \partial x + \partial u_x / \partial y \end{Bmatrix} \tag{2.3}$$

where ρ, E, v and η are density, Young's modulus, Poisson's ratio and damping constant, respectively, and (u_x, u_y) denote x- and y-displacements, respectively.

To simulate the fracture process due to dynamic loading, the incremental displacement form of a dynamic finite element method is used based on the Newmark-β method (Newmark, 1959). The spatially discretized form of with respect to time t is:

$$\boldsymbol{M}\ddot{\boldsymbol{u}}(t) + \boldsymbol{C}\dot{\boldsymbol{u}}(t) + \boldsymbol{K}\boldsymbol{u}(t) = \boldsymbol{f}(t) \tag{2.4}$$

where the vector $\boldsymbol{f}(t)$ is the externally applied loads to each node, the vectors $\ddot{\boldsymbol{u}}(t)$, $\dot{\boldsymbol{u}}(t)$ and $\boldsymbol{u}(t)$ denote the acceleration, velocity, and displacement at each node, and $\boldsymbol{M}$, $\boldsymbol{C}$, and $\boldsymbol{K}$ denote the mass, viscous, and stiffness matrices. Adopting the 3-point triangular element consisting of nodes denoted by i, j, k, these matrices for each element are expressed by following forms:

$$\boldsymbol{K} = h\iint_S \boldsymbol{B}^T \boldsymbol{D}\boldsymbol{B} dxdy \tag{2.5}$$

$$\boldsymbol{C} = \eta \boldsymbol{K} \tag{2.6}$$

$$\boldsymbol{M} = 2\rho h \iint_S \boldsymbol{N}^T \boldsymbol{N}\, dxdy \tag{2.7}$$

where h is the thickness of the element and $\iint_S dxdy$ is the area integral in the element. The matrices $\boldsymbol{B}$ and $\boldsymbol{N}$ are the strain-displacement transform matrix and the matrix consisting of the shape functions, respectively, and these are given as:

$$\boldsymbol{B}(x,y) == \begin{bmatrix} \frac{\partial N_i(x,y)}{\partial x} & 0 & \frac{\partial N_j(x,y)}{\partial x} & 0 & \frac{\partial N_k(x,y)}{\partial x} & 0 \\ 0 & \frac{\partial N_i(x,y)}{\partial y} & 0 & \frac{\partial N_j(x,y)}{\partial y} & 0 & \frac{\partial N_k(x,y)}{\partial y} \\ \frac{\partial N_i(x,y)}{\partial y} & \frac{\partial N_i(x,y)}{\partial y} & \frac{\partial N_j(x,y)}{\partial y} & \frac{\partial N_j(x,y)}{\partial y} & \frac{\partial N_k(x,y)}{\partial y} & \frac{\partial N_k(x,y)}{\partial y} \end{bmatrix} \tag{2.8}$$

$$\boldsymbol{N}(x,y) = \begin{bmatrix} N_i(x,y) & 0 & N_j(x,y) & 0 & N_k(x,y) & 0 \\ 0 & N_i(x,y) & 0 & N_j(x,y) & 0 & N_k(x,y) \end{bmatrix} \tag{2.9}$$

$$N_i(x,y) = \frac{(x-x_j)(y_j-y_k)-(y-y_j)(x_j-x_k)}{2S} \qquad (i\rightarrow j\rightarrow k\rightarrow i) \tag{2.10}$$

where N_i, N_j and N_k are the shape functions at the nodes i, j, k, respectively, and S is area of each element.

It is noticed that the area integral in Equation (2.5) is easily calculated because each component of the matrix $\boldsymbol{B}$ is independent of the coordinates (x, y). The area integral in Equation (2.7) is also easily calculated mathematically.

2.2.2 Modeling of tensile fracture

In the DFPA for 2-D plane strain problem, a re-meshing algorithm is used to model the crack propagations, assuming that tensile fractures, i.e., crack initiations, propagations and coalescences, occur at each element boundary. Thus, the cracks are modeled as the separations of each element boundary without changing the shape of elements. At each element boundary, the fracture potential is checked at every time step. The fracture potential is calculated from the ratio of the normal stress and tensile strength at the element boundary. If the fracture potential at

the element boundary is greater than 1, the node between the elements is separated into two nodes.

In rock fracture mechanics, the behavior of the fracture process zone in front of the crack tips can be simulated with a tensile softening curve (*e.g.*, Hillerborg, 1983; Sato *et al.*, 1990; Whittaker *et al.*, 1992). Assuming that the mechanical behavior of a fracture process zone during dynamic crack growth is similar to that in static or quasi-static crack growth, the 1/4 model can be used as an approximate function of the tensile softening curve. Because the cracking and fracture processes are treated as separations of an element, contact problems, *i.e.*, overlapping of the separated elements, may occur due to the perpendicular compression stress applied to the separated elements. The problem is solved iteratively to prevent topological overlapping of each element until the separated elements are in contact with each other. At each iteration, the crack opening displacements at all of the separated elements are checked. In case that the crack opening displacements correspond to the overlapping, contact forces are applied until the crack opening displacements become zero (Bažant and Pfeiffer, 1987).

2.2.3 Modeling of strength distribution

Rock is an inhomogeneous material, and the inhomogeneity plays a significant role in the fracture process. In DFPA, Weibull's distribution (Weibull, 1951) is employed to represent the microscopic strength of rock-like materials. Considering the microscopic strength x_t in a volume V, the cumulative probability distribution $G(V, x_t)$ is:

$$G(V,x_t)=1-exp\left[-\frac{V}{V_0}\left(\frac{x_t}{\bar{x}_t(V_0)}\right)^m \Gamma^m\left(1+\frac{1}{m}\right)\right] \tag{2.11}$$

where Γ is the Gamma function, m is the coefficient of uniformity, V_0 is the reference volume and $\bar{x}_t$ is the mean microscopic tensile strength. Random numbers satisfying Weibull's

distribution are generated to give the spatial distribution of the microscopic strengths in the analysis model.

2.3 DFPA FOR AXISYMMETRIC PROBLEM (DFPA-A)

2.3.1 Finite Element Formulation

A cylindrical body with the single charge hole shown in Fig. 2.1 is considered. The figure is shown by cylindrical coordinate (r, θ, z) where z coincides with the axial direction of the charge hole, and r and θ are polar coordinates at the cross section perpendicular to the z axis. If the domain of interest has axisymmetric property with respect to z axis, u_θ in the displacement field (u_r, u_θ, u_z) becomes zero. Thus, only u_r and u_z need to be considered.

The governing equations in axisymmetric problem are given by following equations.
The equation of motion:

$$\begin{aligned}\frac{\partial \sigma_{rr}}{\partial r}+\frac{\sigma_{rr}-\sigma_{\theta\theta}}{r}+\frac{\partial \sigma_{zr}}{\partial z}&=\rho\frac{\partial^2 u_r}{\partial t^2}\\ \frac{\partial \sigma_{rz}}{\partial r}+\frac{\sigma_{rz}}{r}+\frac{\partial \sigma_{zz}}{\partial z}&=\rho\frac{\partial^2 u_z}{\partial t^2}\end{aligned} \tag{2.12}$$

The constitutive equation of visco-elasticity (visco-elastic stress-strain relation):

$$\begin{Bmatrix}\sigma_{rr}\\ \sigma_{zz}\\ \sigma_{\theta\theta}\\ \sigma_{rz}\end{Bmatrix}=\frac{E}{(1+\nu)(1-2\nu)}\begin{pmatrix}1-\nu & \nu & \nu & 0\\ \nu & 1-\nu & 0 & 0\\ \nu & 0 & 1-\nu & 0\\ 0 & 0 & 0 & \frac{1-2\nu}{2}\end{pmatrix}\begin{Bmatrix}\varepsilon_{rr}+\eta\partial\varepsilon_{rr}/\partial t\\ \varepsilon_{zz}+\eta\partial\varepsilon_{zz}/\partial t\\ \varepsilon_{\theta\theta}+\eta\partial\varepsilon_{\theta\theta}/\partial t\\ \gamma_{rz}+\eta\partial\gamma_{rz}/\partial t\end{Bmatrix} \tag{2.13}$$

The strain-displacement relation:

$$\begin{Bmatrix} \varepsilon_{rr} \\ \varepsilon_{zz} \\ \varepsilon_{\theta\theta} \\ \gamma_{rz} \end{Bmatrix} = \begin{Bmatrix} \partial u_r / \partial r \\ \partial u_z / \partial z \\ u_r / r \\ \partial u_r / \partial z + \partial u_z / \partial r \end{Bmatrix} \tag{2.14}$$

where ρ, E and v are the density, Young's modulus and Poisson's ratio, respectively.

By discretizing the domain of interest by triangular ring elements denoted by node (i, j, k), it can be reduced to the FEM mesh shown in Fig. 2.2.

The spatially discretized form of equation of motion is given as:

$$\boldsymbol{M}\ddot{\boldsymbol{u}}(t) + \boldsymbol{C}\dot{\boldsymbol{u}}(t) + \boldsymbol{K}\boldsymbol{u}(t) = \boldsymbol{f}(t) \tag{2.15}$$

where the vector $\boldsymbol{f}(t)$ is the externally applied loads, the vectors $\ddot{\boldsymbol{u}}(t)$, $\dot{\boldsymbol{u}}(t)$ and $\boldsymbol{u}(t)$ denote the acceleration, velocity, and displacement, and $\boldsymbol{M}$, $\boldsymbol{C}$ and $\boldsymbol{K}$ are mass matrix, viscosity matrix and stiffness matrix, respectively. In case of the ring element, these matrices are given as:

$$\boldsymbol{K} = 2\pi \iint_S \boldsymbol{B}^{\boldsymbol{T}}(r,z)\boldsymbol{D}\boldsymbol{B}(r,z) r dr dz \tag{2.16}$$

$$\boldsymbol{C} = \eta \boldsymbol{K} \tag{2.17}$$

$$\boldsymbol{M} = 2\pi\rho \iint_S \boldsymbol{N}^T(r,z)\boldsymbol{N}(r,z) r dr dz \tag{2.18}$$

where $\iint_S r dr dz$ is the area integral in a ring element. Matrices $\boldsymbol{B}$ and $\boldsymbol{N}$ are expressed as follows:

$$\mathbf{B}(r,z) = \begin{bmatrix} \frac{\partial N_i(r,z)}{\partial r} & 0 & \frac{\partial N_j(r,z)}{\partial r} & 0 & \frac{\partial N_k(r,z)}{\partial r} & 0 \\ 0 & \frac{\partial N_i(r,z)}{\partial z} & 0 & \frac{\partial N_j(r,z)}{\partial z} & 0 & \frac{\partial N_k(r,z)}{\partial z} \\ \frac{N_i}{r} & 0 & \frac{N_j}{r} & 0 & \frac{N_k}{r} & 0 \\ \frac{\partial N_i(r,z)}{\partial z} & \frac{\partial N_i(r,z)}{\partial r} & \frac{\partial N_j(r,z)}{\partial z} & \frac{\partial N_j(r,z)}{\partial r} & \frac{\partial N_k(r,z)}{\partial z} & \frac{\partial N_k(r,z)}{\partial r} \end{bmatrix} \tag{2.19}$$

$$\boldsymbol{N}(r,z)=\begin{bmatrix} N_i(r,z) & 0 & N_j(r,z) & 0 & N_k(r,z) & 0 \\ 0 & N_i(r,z) & 0 & N_j(r,z) & 0 & N_k(r,z) \end{bmatrix} \tag{2.20}$$

$$N_i(r,z)=\frac{(r-r_j)(z_j-z_k)-(z-z_j)(r_j-r_k)}{2S} \quad (i\rightarrow j\rightarrow k\rightarrow i) \tag{2.21}$$

where N_i, N_j and N_k are the shape functions at the nodes i, j, k, respectively, and S is area of each ring element.

From these equations, it is noticed that the matrix $\boldsymbol{B}$ contains functions of r in the case of axisymmetric problem. Then the area integral in Equation (2.16) needs to be computed by standard 3-point Gaussian quadrature (e.g., Cowper 1973; Hillion 1977; Laursen and Gellert 1987; Ma *et al*. 1996), while the area integral in Equation (2.18) is evaluated by explicit integration. With the application of new-mark β method for time discretization, nodal accelerations, velocities and displacements as well as stresses and strains can be calculated.

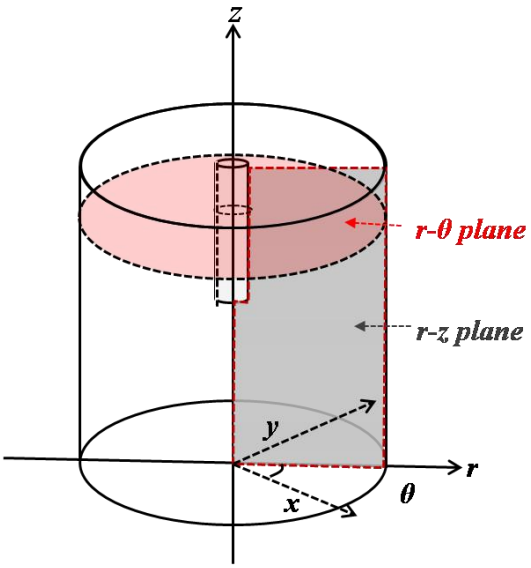

Figure 2.1 Axisymmetry with respect to *z*-axis

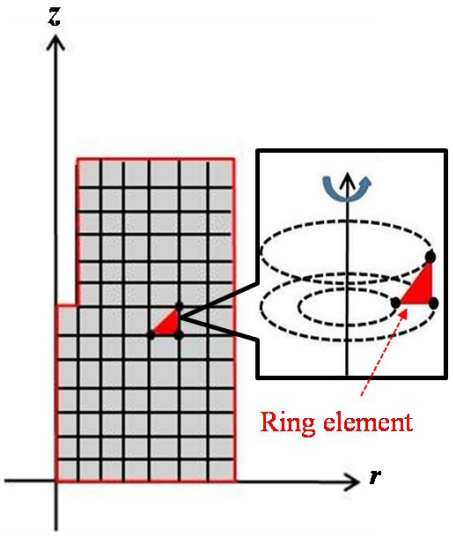

Figure 2.2 Finite element discretization

2.3.2 Modeling of tensile fracture

In the axisymmetric problem, there are three principal directions, i.e. one component is in *r*-θ plane and the other two components are in *r*-*z* plane. Thus, the number of corresponding principal stresses is 3, and therefore fractures in three directions need to be considered. The

treatment of fracturing in *r*-*z* plane and *r*-θ plane is individually described as follows.

(a) Tensile fracture in *r*-*z* plane

For the tensile fracture in *r*-*z* plane, inter element cracking method (Xu and Needleman, 1994; Camacho *et al*, 1996; Ortiz and Pandolfi, 1999; Song. *et al*., 2008, 2009; Kaneko *et al.*, 1995) is used where the crack initiation, propagation and coalescence are expressed by element separations when the induced stress normally acting on element-boundary exceeds the given tensile strength of the boundary as shown in Fig. 2.3. Once the crack is initiated, non-linear crack opening behavior due to the existence of fracture process zone (FPZ) near the crack tip is considered, and the bi-linear model of cohesive law characterized by cohesive traction and crack opening displacement (COD) shown in Fig. 2.4 is used.

(b) Tensile fracture in *r*-θ plane

Tensile fracture in *r*-θ plane is also taken into account in the axisymmetric problem. However, because u_θ is zero in this class of problem, the cohesive law in Fig. 2.4 cannot be applied directly. Alternatively, stress-strain relation in each element to express the decohesion of crack surfaces in *r*-θ plane is used as shown in Fig. 2.5. In this approach, stress (σ_θ)-strain (ε_θ) relation is expressed by linear elastic behavior when the induced stress level is below the given tensile strength, then, after the stress exceeds the given tensile strength, the stress-strain relation corresponding to the decohesion process characterized by bi-linear model of cohesive law is used instead of COD. To reasonably evaluate strains, ε_1 and ε_2 in the decohesion process, a fracture pattern assuming a cross section of *r*-θ plane in Fig. 2.1 with recourse to DFPA for 2-D strain plain problem can be utilized. An exemplary fracture pattern is shown in Fig. 2.5 and five predominant cracks are obtained in this figure. In this case, the whole domain is equally divided into five subdomains, each of which includes one predominant crack, and crack opening strain (COS) defined by the ratio of COD to arch length L of subdomains can be approximately determined as shown in Fig. 2.6. By generalizing the above example, L is computed by following equation:

$$L = 2\pi r / n \tag{2.22}$$

where n is number of the predominant cracks. Following this concept, ε_1 and ε_2 can be computed by W_1/L and W_2/L, respectively, in which W_1 and W_2 in Figure 2.4 are used.

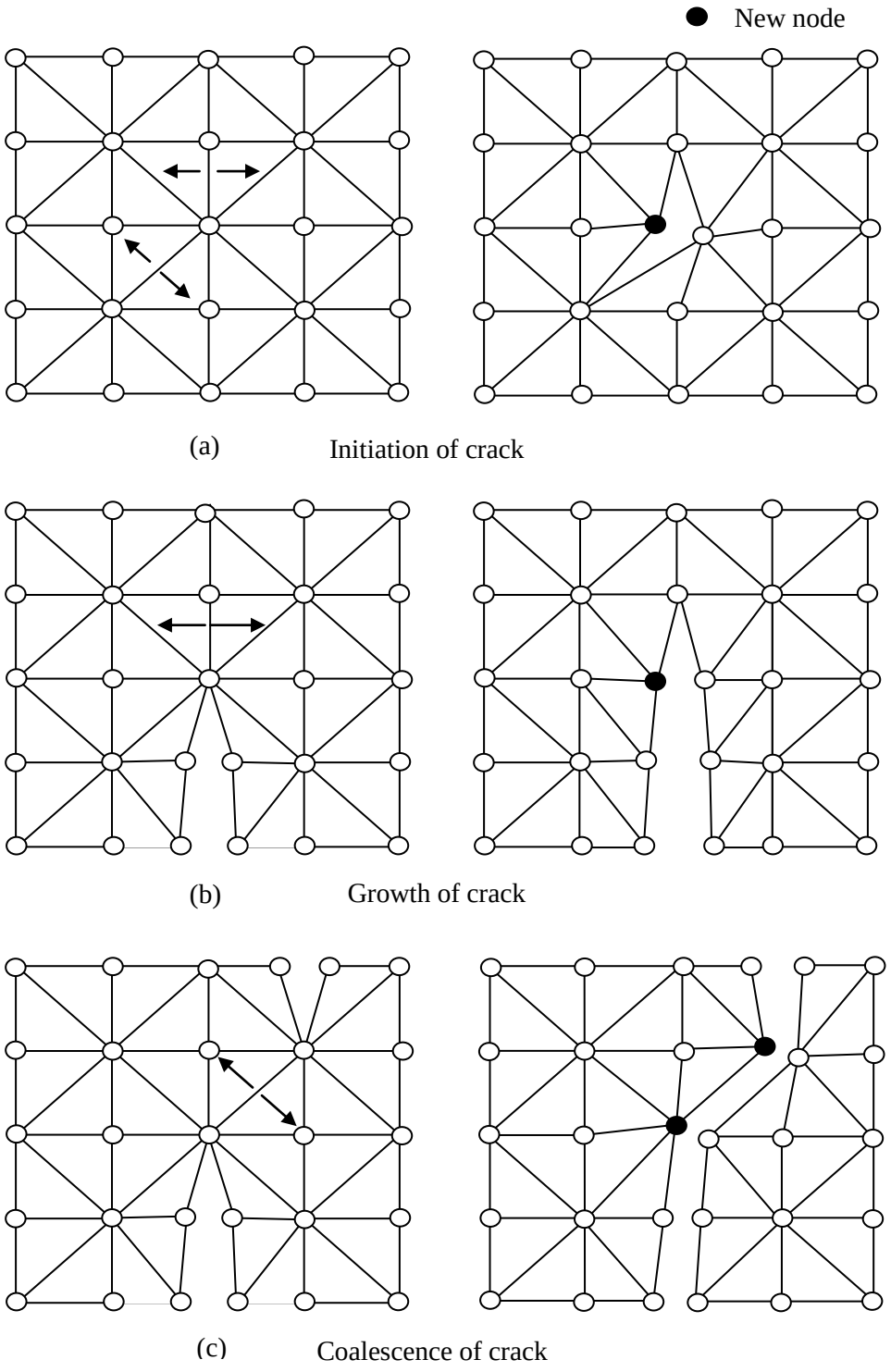

Figure 2.3 Remeshing procedures for the tensile fracture in *r*-*z* plane.

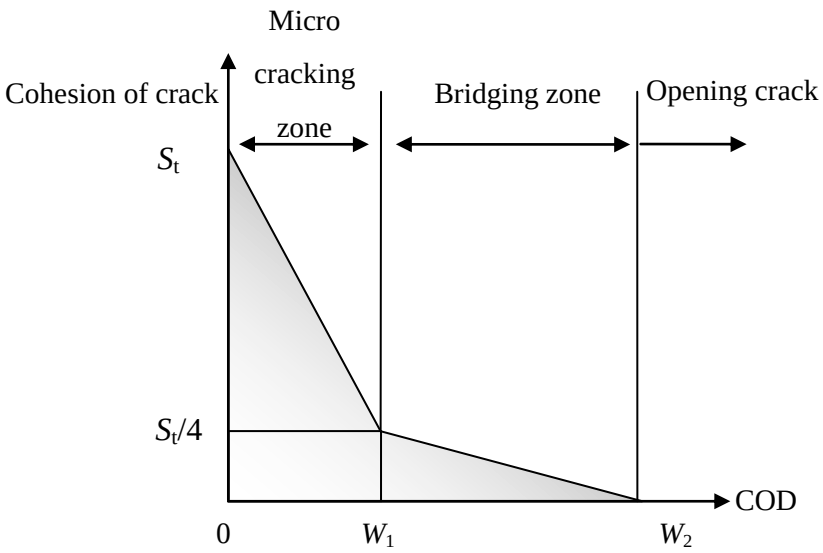

Figure 2.4 Tensile softening curve for the FPZ.

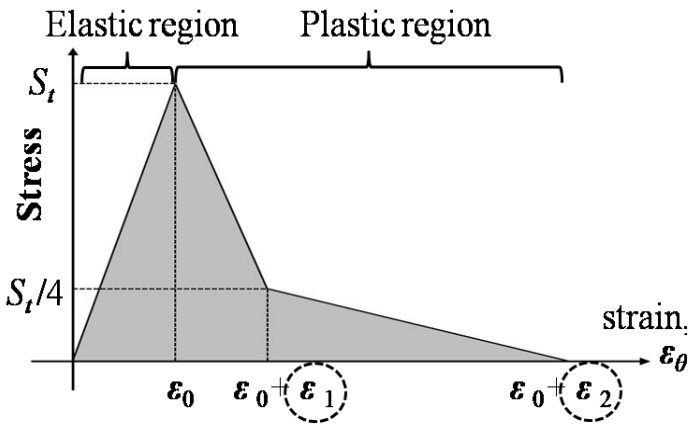

Figure 2.5 Tensile softening curve in r-θ plane.

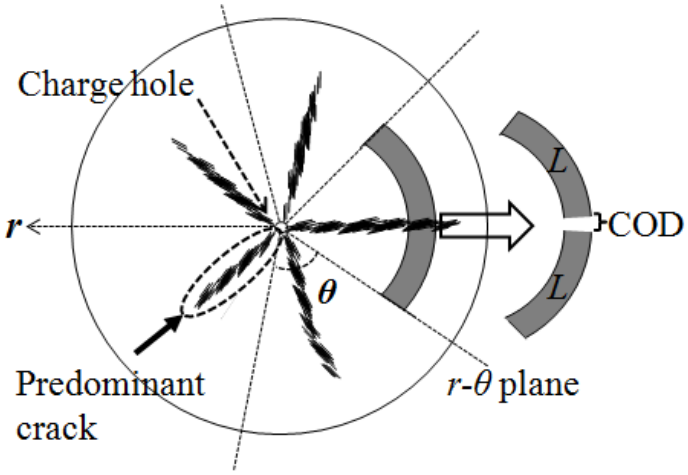

Figure 2.6 An interpretation of crack propagation in r-θ plane.

2.3.3 Modeling of strength distribution

As an extension of DFPA for 2-dimension plain strain problem, microscopic tensile strength distribution in the material is expressed by Weibull's distribution characterized by coefficient of uniformity, m. However, the concept of heterogeneity in the axisymmetric problem shows a contradiction in that the axisymmetry with respect to z axis requires the strength distribution to be axisymmetric in the r-z planes for each θ. The influence of heterogeneity on numerical results will be discussed in detail in Chapter 3.

2.4 CONCLUDING REMARKS

In this chapter, DFPA for 2-D plane strain problem was reviewed and DFPA-A was proposed for the simulation of breakage of concrete pile head. In particular, the DFPA for 2-D plane strain problem can be useful for the simulation of breakage of rectangular shaped concrete pile head due to blasting and is applied in Chapter 5. On the other hand, the DFPA-A can be useful for the simulation of breakage of cylindrical concrete pile head in which both the crack

propagation from the bottom part of cylindrical charge hole due to blasting and the effectiveness of crack arrester can be investigated.

Through the formulation of DFPA-A, it was pointed out that two kinds of tensile fracturing, i.e., the tensile fractures within *r*-*z* plane and normal to *r*-θ plane in the cylindrical coordinate must be taken into account. Following DFPA for 2-D plane strain problem, inter cracking method was used in the modeling of the tensile fracture within *r*-*z* plane to express crack initiation, propagation and coalescence and the cohesive law was adopted to simulate the nonlinear crack opening behavior due to the existence of fracture process zone near the crack tip. In the modeling of the tensile fracture normal to *r*-θ plane, the stress-strain relation in each element was used to express the decohesion of crack surface and a concept of Crack Opening Strain (COS) was proposed. Contrary to the DFPA for 2-D plane strain problem, the DFPA-A is newly proposed method in this dissertation and thus, the DFPA-A code must be developed and its implementation and applicability are discussed in Chapter 3. Then, the DFPA-A is applied to the simulation of breakage of cylindrical concrete pile head in Chapter 4.

BIBLIOGRAPHY

1) Bažant, Z. P., and Pfeiffer, P., 1987, Fracture energy of concrete, Katherine and Bryant Mather International Conference on Concrete Durability, pp.89-109.
2) Camacho, G. and Ortiz, M., 1996, Computational modelling of impact damage in brittle materials, Int J Solids Struct, Vol.33, pp.2899-2938.
3) Cho, S.H., 2003, Dynamic fracture process analysis of rock and its application to fragmentation control in blasting, Doctor dissertation, Hokkaido University, Japan.
4) Cho, S.H., Ogata, Y. and Kaneko, K., 2003a, Strain rate dependency of the dynamic tensile strength of rock. Int. J. Rock. Mech. Min. Sci., Vol.40, No.5, pp. 763-777.
5) Cho, S.H., Nishi, M., Yamamoto, M. and Kaneko, K., 2003b, Fragment size distribution in blasting, Mater. Trans, Vol.44, No.5, pp.951-956.
6) Cho. S.H. and Kaneko, K., 2004, Influence of the applied pressure wave form on the dynamic fracture processes in rock, Int. J. Rock Mech.Min. Sci., Vol. 41, pp.771-784.
7) Cho, S.H., Mohanty. B., Ito, M., Nakamiya, Y., Owada, S., Kubota, S., Ogata, Y., Tsubayama, A., Yokota, M. and Kaneko, K., 2006, Dynamic fragmentation of rock by high-voltage pulses, Int. Proceedings of 41st US symposium on rock mechanics, Curran Associates, Inc., 06-1118.
8) Cho, S.H., Nakamura, Y., Mohanty. B, Yang. H.S, Kaneko. K, 2008, Numerical study of fracture plane control in laboratory-scale blasting, Engineering Fracture mechanics, Vol. 75(13), pp.3966-3984.
9) Cowper. G.R, 1973, Gaussian quadrature formulas for triangles, Int. J. Num. Meth. Eng., Vol.7, No.3, pp. 405-408.
10) Fukuda, D., Moriya, K., Kaneko, K., Sasaki, K., Sakamoto. R, Hidani. K, 2012, Numerical simulation of the fracture process in concrete resulting from deflagration phenomena, Int. J. Fract, Vol. 180(2), pp. 163-175.
11) Hillerborg, A., 1983. Analysis of a single crack. In, Fracture Mechanics of Concrete, F.H. Whittman (ed.), Elsevier, Amsterdam, Netherlands, pp. 223-249.

12) Hillon, P., Numerical integration on a triangle, Int. J. Numer. Meth. Eng., Vol.11, pp.797-815.
13) Laursen, M.E. and Gellert, M., 1978, Some criteria for numerically integrated matrices and quadrature formulas for triangles, Int. J. Numer. Meth. Eng., Vol.12, pp. 67-76.
14) Ma, J., Rokhlin, V. and Wandzura, S., 1996, Generalized Gaussian quadrature rules for systems of arbitrary functions, SIAM J. Numer. Anal., Vol.33, No.3, pp.971-996.
15) Newmark, N.M., 1959, A Method of Computation for Structural Dynamics, Proc. ASME, EM-3, pp. 67-94.
16) Ortiz, M. and Pandolfi, A., 1999, A class of cohesive elements for the simulation of three-dimensional crack propagation, Int J Numer Meth Eng, Vol.44, pp.1267-1282.
17) Sassa, K. and Ito, I., 1972, Journal of The Society of Materials Science, Vol.21, pp.123-129 [in Japanese].
18) Sato, K., Awayama, H., Hashida, T., and Takahashi, H., 1990, Determination of strain-softening curve and fracture toughness of granite, Trans. JSME(A), Vol.56, No.526, pp.1400-1405.
19) Song, J.H. Wang, H. and Belytschko, T., 2008, A comparative study on finite element methods for dynamic fracture, Comput. Mech. Vol.42, pp.239-250.
20) Song, J.H. and Belytschko, T., 2009, Cracking node method for dynamic fracture with finite elements, Int. J. Numer. Meth. Eng., Vol.77, pp.360-385.
21) Kaneko. K., Matsunaga. Y. and Yamamoto. M., 1995. Fracture mechanics analysis of fragmentation process in rock blasting. J. Japan Exp. Soc., Vol. 58, No.3, pp. 91-99 [in Japanese].
22) Weibull, W., 1951, A statistical distribution function of wide applicability, J. Appl. Mech., Vol.18, pp.293-297.
23) Whittaker, B.N., Singh, R.N., and Sun, G. 1992. Rock Fracture Mechanics. Design and Application. Elsevier.
24) Xu, X.P. and Needlman, A., 1994, Numerical simulation of fast crack growth in brittle solids, J. Mech. Phys. Solids., Vol.42, pp. 1397-1434.

25) Yamamoto, M., Ichijo, T., Inaba, T., Morooka, K., and Kaneko, K., 1999, Experimental and theoretical study on smooth blasting with electronic delay detonators, Int. J. of Rock Fragmentation by Blasting, Vol.3, No.1, pp.3-24.

CHAPTER 3

APPLICATION OF DYNAMIC FRACTURE PROCESS ANALYSIS FOR AXISYMMETRIC PROBLEM

3.1 INTRODUCTION

For the simulation of breakage of concrete pile head by blasting envisioned in this desertion, 3-dimentional (3-D) fracturing process analysis is indispensable because investigation regarding the control of crack propagation toward the depth of charge hole, i.e. the minimization of damage in the remaining part of concrete pile due to the concrete pile head removal, is impossible by 2-dimentional (2-D) dynamic fracturing process analysis (DFPA) code for plane strain problem (e.g., Kaneko *et al*. 1995; Yamamoto *et al*. 1999; Cho 2003; Cho *et al*. 2003a,b; Cho and Kaneko 2004; Cho *et al*. 2006, 2008; Fukuda *et al*. 2013). However, as pointed out in Chapter 2, the fracturing process in the case of concrete pile head due to blasting a cylindrical charge can be analyzed by regarding the problem as axisymmetric (Sassa and Ito, 1972). For this purpose, the methodology of DFPA for axisymmetric problem (DFPA-A) was proposed in Chapter 2 in which two kinds of tensile fractures i.e., the crack initiation, propagation and coalescence tensile fractures in *r-z* plane and *r-z* plane were modeled with the consideration of nonlinear decohesion process of crack surfaces and material heterogeneity. The DFPA-A can be useful for the simulation of breakage of cylindrical concrete pile head in which both the crack propagation from the bottom part of cylindrical charge hole due to blasting and effectiveness of crack arrester, i.e. the target of investigation in Chapter 4, can be investigated. However, the

numerical simulator based on the DFPA-A has not been developed. In addition, country to 2-D DFPA code, the applicability of DFPA-A has not been verified yet.

In this chapter, DFPA-A code is developed and applicability of the DFPA-A is verified through the implementation of the fracturing simulation assuming a concrete pile by blasting a cylindrical charge. Through the discussion of fracturing mechanism in dynamic breakage of a concrete pile, the importance of crack arrester investigated in Chapter 4 is also introduced.

3.2 MODEL DESCRIPTION

A cylindrical concrete having a single cylindrical charge hole is considered and the information of model geometry is shown in Fig. 3.1. Then, the consideration of axisymmetry with respect to the axial direction of charge hole leads to the FEM mesh shown in Fig. 3.2. The analysis model has free surfaces in the upper, bottom and right boundaries of the model. Each element size is set to be small enough to avoid the mesh dependency of crack path. The total element number and initial total nodal number are 69364 and 35000, respectively. The physical properties of concrete used in the analysis are shown in Table 1. To generate borehole pressure, a general form of the applied pressure pulse function (Duvall 1953; Ito 1968) is used:

$$P(t) = P_0\{1 - \exp(-\alpha t)\} \tag{3.1}$$

where $P(t)$ is the pressure at time t, P_0 donates the peak pressure value, and α is constant. As an example, Fig. 3.3 shows the applied pressure wave form with its rise time of 138 μs when $\alpha = 10^4$.

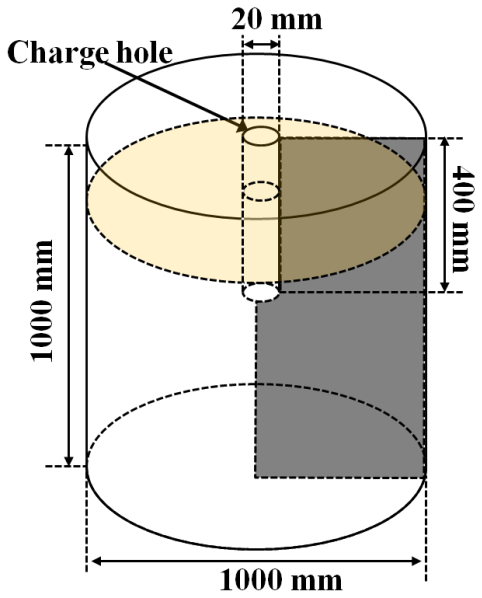

Figure 3.1 Model of a cylindrical concrete specimen with a cylindrical charge hole.

Table 3.1 Physical properties of concrete.

Properties	Value
Density (kg/m^3)	2200
P-wave velocity (m/s)	4000
S-wave velocity (m/s)	2450
Young's modulus (GPa)	31.7
Poisson's ratio	0.2
Mean tensile strength (MPa)	6
Fracture energy (Pa m)	96

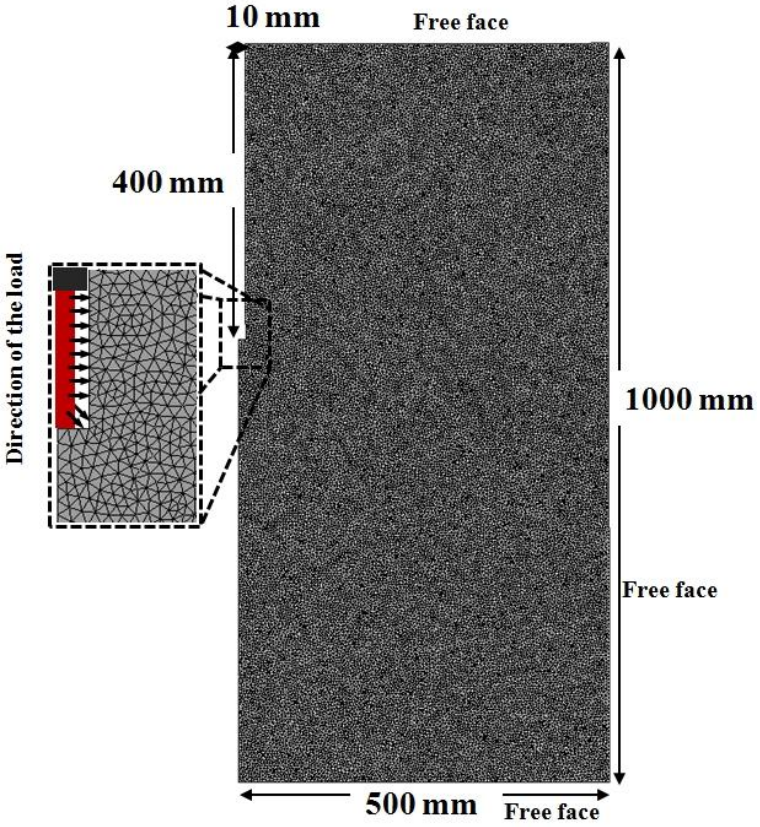

Figure 3.2 Description of Finite element mesh corresponding to Fig.3.1.

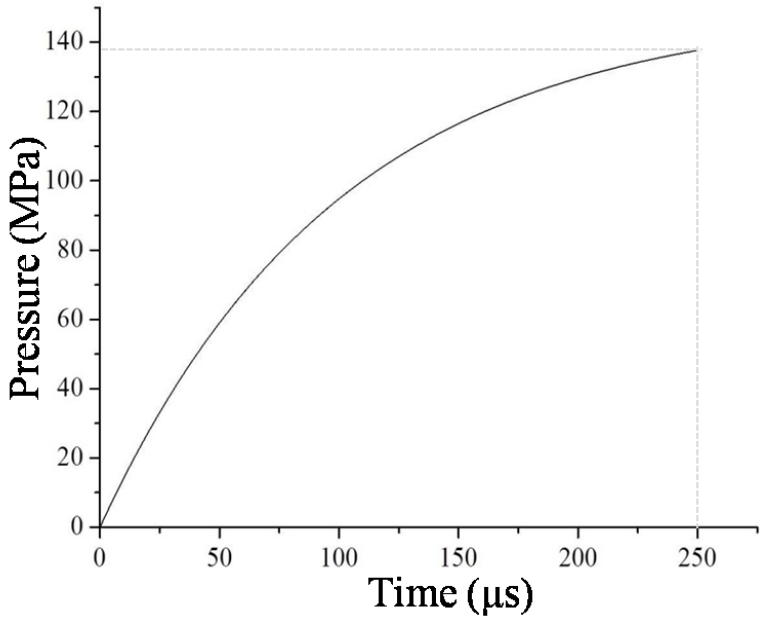

Figure 3.3 Pressure-time curve for applied pressure to charge hole in case of rise time of 138 μs ($\alpha = 10^4$).

3.3 NUMERICAL RESULTS

3.3.1 Fracture process in rock-like material with a cylindrical charge hole

In Fig. 3.4, a result of fracture process under m = 30, i.e. relatively homogeneous condition, from time t = 10 to 250 μs is shown at the time interval of 10μs. The value of n, the number of predominant cracks introduced in Chapter 2 to reasonably calculate the crack opening strain, is 5. The solid black lines are tensile fractures initiated and extended in r-z plane (hereafter, r-z fractures), and red colored regions correspond to the tensile fractures in r-θ plane (hereafter, r-θ fractures). Around t = 100 μs, the r-z and r-θ fractures initiated from the side wall of the charge hole are observed. It is also observed that the r-z fractures extended obliquely downward from the bottom of the charge hole. While minor extensions of the r-z fractures from the side wall of charge hole is found, major extension of both the oblique r-z fractures and r-θ fractures are found where the r-θ fractures only occur above the oblique r-z fractures and the most significant r-θ fractures are found on the upper surface of the model.

3.3.2 Influence of the bottom shape of charge hole

Because it is possible that the existence of corner around the bottom of the charge hole induces stress concentration, the effect of bottom shape of the charge hole on the resultant fracture pattern is investigated. For this purpose, four models similar to that in Fig.3.1 are considered where only the shape of the bottom corner of charge hole in each model is changed in terms of curvature radius, 10 mm, 5 mm, 2.5 mm and 0, respectively. In Fig. 3.5, the resultant fracture patterns for the four models are shown corresponding to t = 250 μs. These results show that almost same fracture patterns are obtained and thus the oblique r-z fractures from the bottom of charge hole are always initiated irrespective of considered curvature radii and thus

indicate that propagation of the oblique *r-z* fracture from the bottom of charge hole does not depend on the shape of bottom corner of charge hole but is the intrinsic fracture pattern in blasting a concrete pile by a cylindrical charge.

For the mechanism of initiation and propagation of the *r-z* fractures extending obliquely downward, it can be explained in terms of the displacement distribution around the charge hole. Considering the time just after the initiation in the current model, as shown in Fig. 3.6, the special distribution of displacement along *r* direction, u_r, at a particular distance from the axis of charge hole can be considered as almost constant at the height roughly between top and bottom charge hole. In this region, $\partial u_r/\partial z$ becomes zero. On the other hand, $\partial u_r/\partial z$ no longer is zero toward the region below the bottom corner of charge hole. Considering that the shear strain γ_{rz} is given by sum of $\partial u_r/\partial z$ and $\partial u_z/\partial r$ as well as the fact that u_z can be approximately zero around this region, the non- negligible γ_{rz}, and thus shear stress τ_{rz} is induced around the bottom corner of charge hole. Then, in terms of principal stress, this τ_{rz} can be interpreted from the coupling of principal compressive and tensile stresses as shown in the figure. Therefore, this principal tensile stress can cause the *r-z* fractures extending obliquely downward.

3.3.3 Influence of heterogeneity

As pointed out in Chapter 2, the concept of heterogeneity in the axisymmetric problem shows a contradiction in that the axisymmetry with respect to *z* axis requires the strength distribution to be axisymmetric in the *r-z* planes for each θ. To investigate this problem, in Fig. 3.7, the resultant fracture patterns for the cases of m = 30, 10 and 5 under the same model geometry are shown corresponding to t = 250 μs in which fixed value of n is used. These results clearly show that quite similar fracture patterns are obtained and thus the influence of heterogeneity has minor role on the fracture pattern in the *r-z* planes.

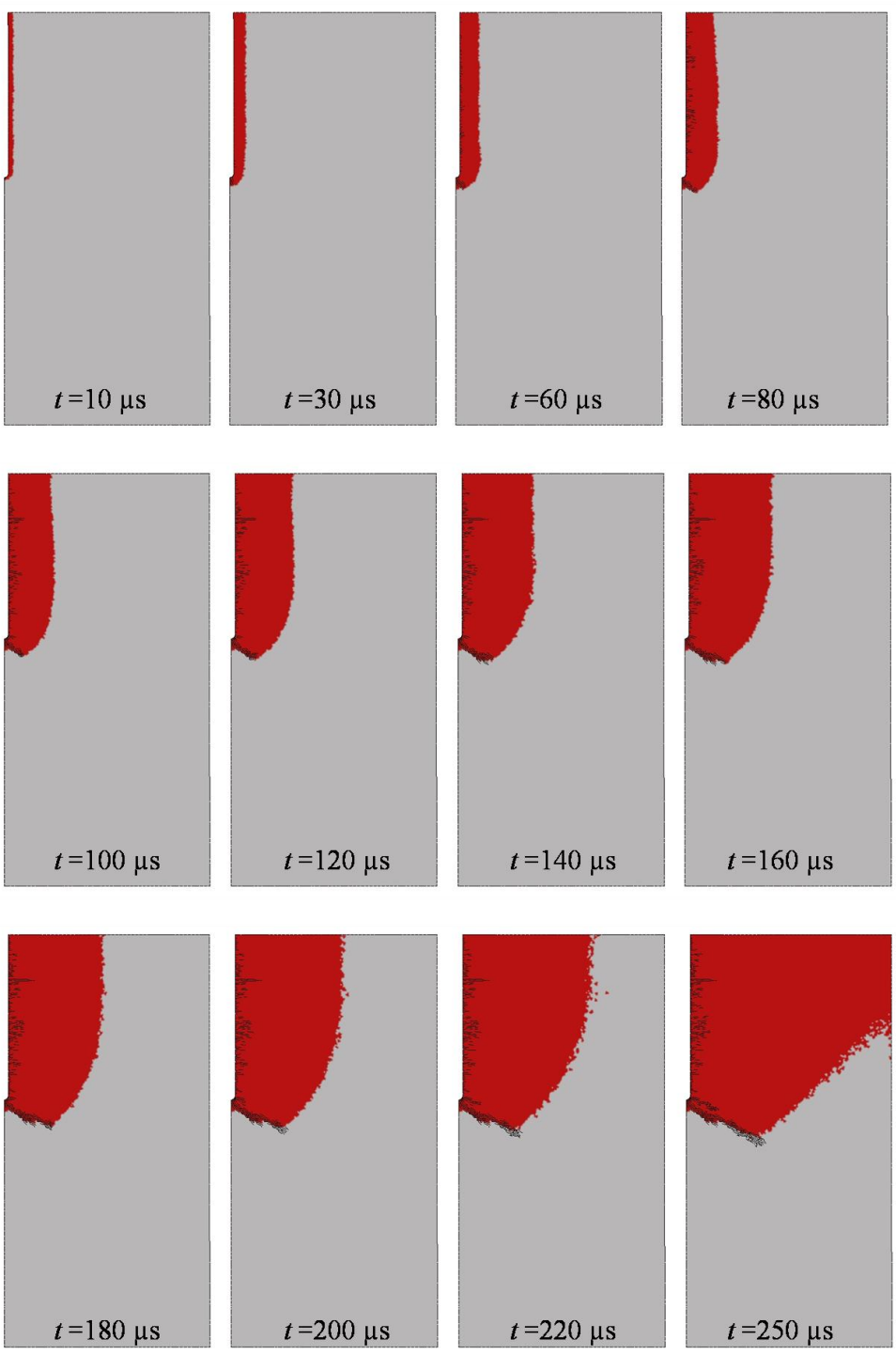

Figure 3.4 Results of fracture process (m = 30, n = 5)

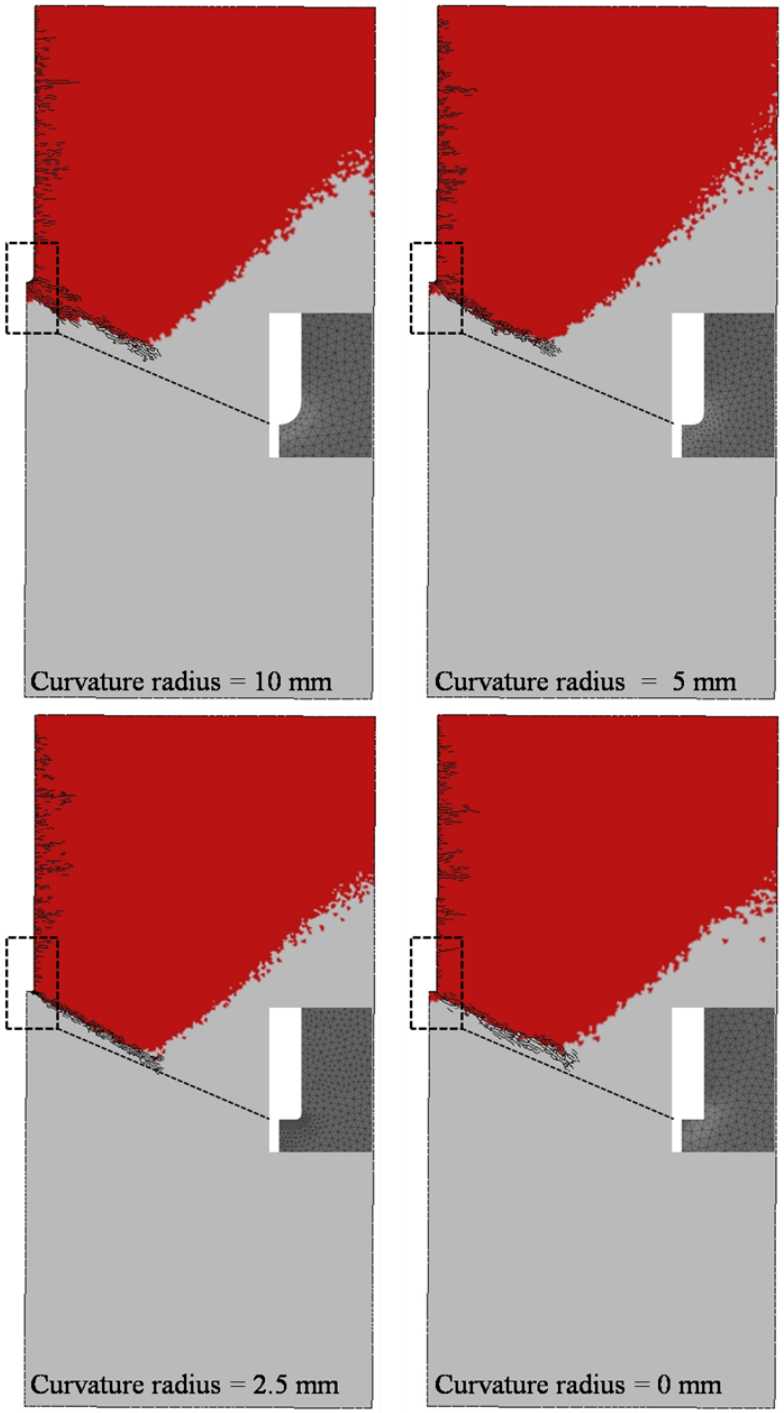

Figure 3.5 Influence of curvature radius of bottom corner of charge hole on resultant fracture pattern (m =30)

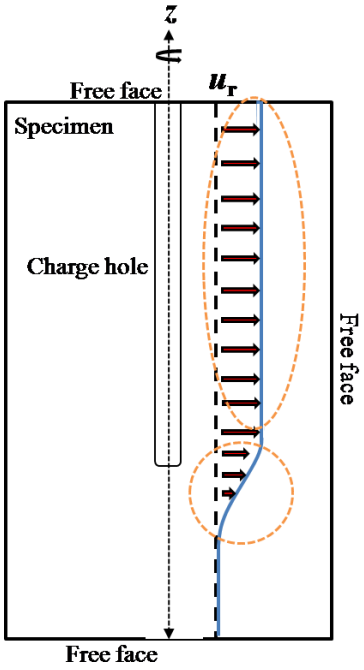

Figure 3.6 Mechanism of initiation and propagation of oblique *r-z* fractures from bottom corner of charge hole.

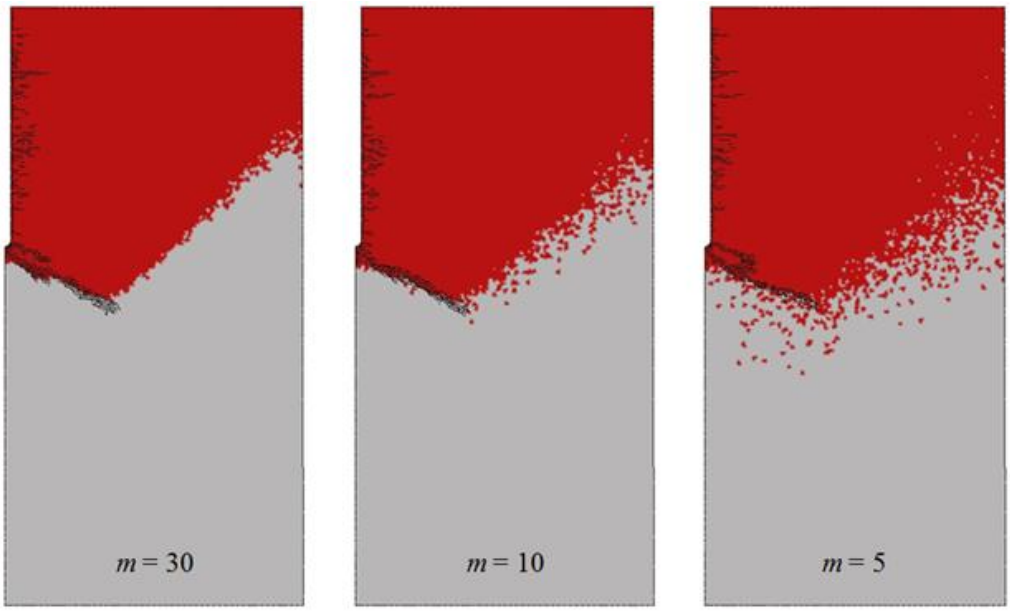

Figure 3.7 Influence of heterogeneity on resultant fracture pattern (n = 5).

3. 4 DISCUSSION

Based on the results obtained in Subsection 3.2, the general resultant 3-D fracture pattern could become the one shown in Fig. 3.8 consisting of predominant *r-θ* fractures from the wall and oblique *r-z* fractures from the bottom corner of charge hole. Considering that the assumption of decohesion in *r-θ* fractures is made based on the propagation of predominant cracks from the charge hole, the *r-θ* fractures become 5 predominant radial cracks as shown in red color and the *r-z* fractures become the conical shaped crack as shown in blue color. The result obtained here shows good agreement with usually observed in rock splitting. Thus proposed simulation method can be useful for the analysis of fracture process in blasting a concrete pile by a cylindrical charge.

The fracture processes obtained from DFPA for plane strain problem and DFPA-A are also compared assuming the same applied load as in Equation (3.1) and physical properties as in Table 1. The result is shown in Fig. 3.9 where one of the radially propagating predominant tensile fractures obtained by DFPA for plane strain problem shown in black color is compared with *r-θ* fracture propagation obtained from the DFPA-A shown in red color. The comparison of both analyses shows good agreement between propagation velocities of radially propagating predominant tensile fractures and the *r-θ* fracture simulated by DFPA for plane strain problem and DFPA-A, respectively. Considering the applicability and precision of DFPA for plane strain problem has been already validated (e.g., Kaneko *et al*. 1995; Yamamoto *et al*. 1999; Cho 2003; Cho *et al*. 2003a,b; Cho and Kaneko 2004; Cho *et al*. 2006, 2008; Fukuda *et al*. 2013), this result shows the validity of the DFPA-A code.

It also could give the insight for the range in which plane strain condition is applicable. From above result of Fig. 3.9, it is indicated that DFPA for 2-D plane strain problem is useful to estimate the propagation of the radial cracks from the charge hole in the region between the mouth and the end of charge hole except for the vicinity of the end. Furthermore, it is indicated that the DFPA-A is indispensable to estimate the propagation of conical cracks from the bottom corner of charge hole.

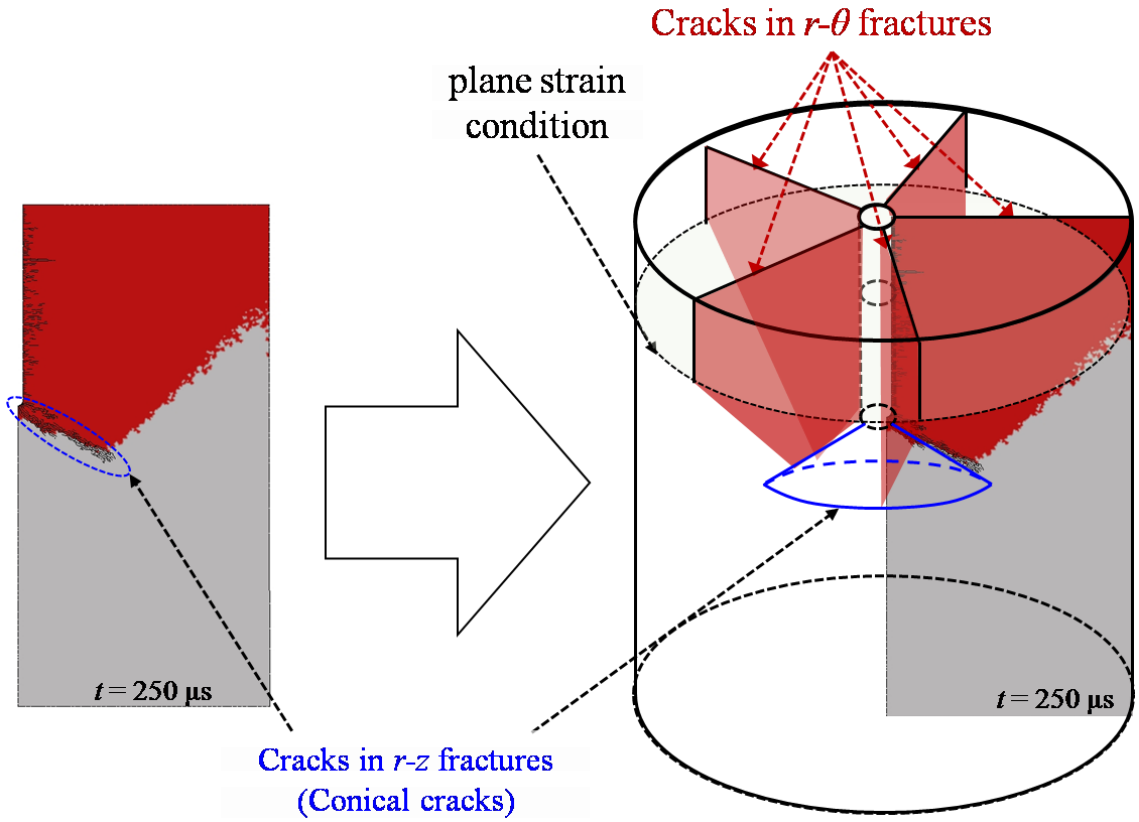

Figure 3.8 3-D fracture pattern of a cylindrical concrete specimen due to blasting a cylindrical charge (t = 250 μs).

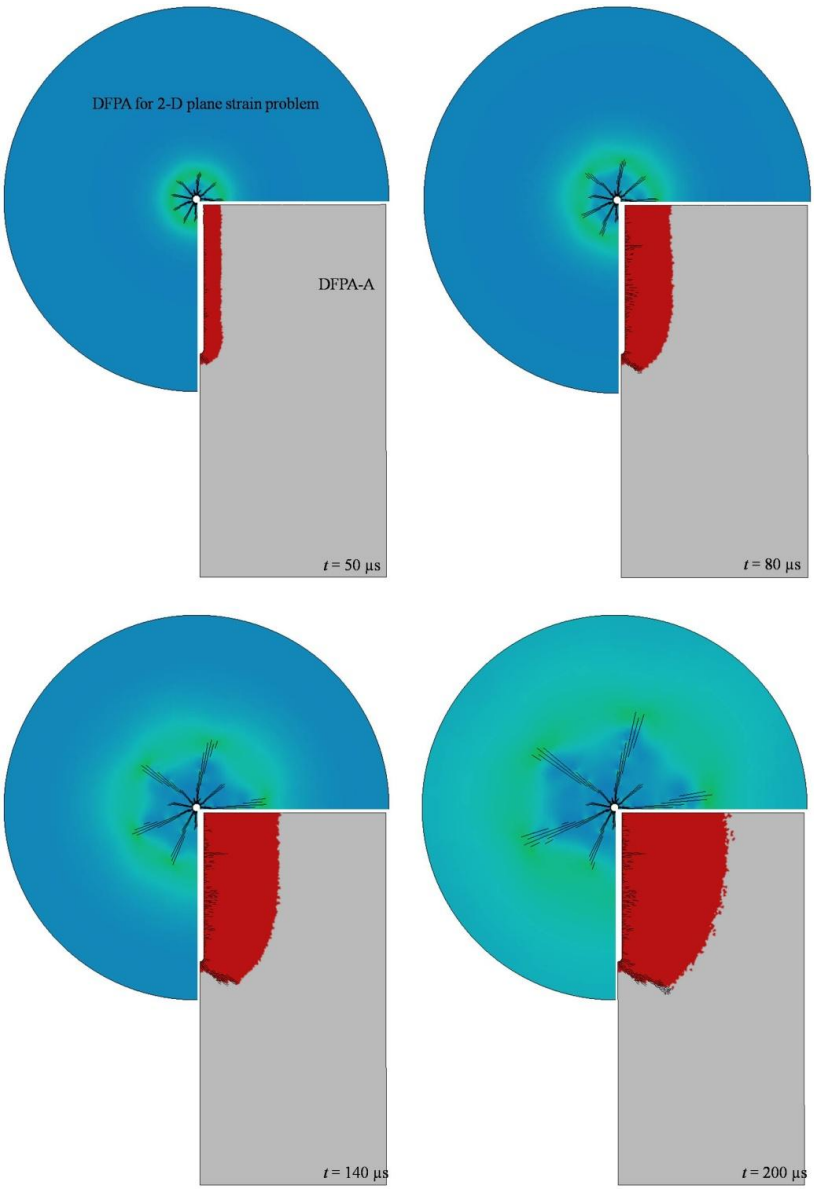

Figure 3.9 Comparison of result in DFPA for 2-D plane strain problem and DFPA-A.

3. 6 CONCLUDING REMARKS

In this chapter, the DFPA-A code was developed and its implementation and applicability are investigated. In the DFPA-A, the conical crack pattern formed from the bottom

of charge hole as well as predominant cracks radially extending from the charge hole were successfully simulated, which agreed with generally obtained fracture pattern from dynamic splitting experiment. Additionally, the DFPA-A gives harmonic fracture patterns compared to those obtained by using DFPA for plane strain problem, which shows the validity of the proposed DFPA-A.

By applying the DFPA-A to the fracturing simulation assuming a concrete pile by blasting a cylindrical charge, it was pointed out that the initiation and propagation of the oblique tensile fracturing, i.e. conical cracks, from the bottom corner of charge hole is inevitable. Because one of the main purposes of this dissertation is to investigate the controlled blasting of concrete pile head by dynamic breakage system proposed by Nakamura et al. (2009) in which the damage to the remaining concrete pile is expected to be minimized. From this aspect, prevention and control of the conical cracks by such as crack arrester is of considerable importance, which is discussed in Chapter 4.

BIBLIOGRAPHY

1) Cho, S.H., 2003, Dynamic fracture process analysis of rock and its application to fragmentation control in blasting, Doctor dissertation, Hokkaido University, Japan.
2) Cho, S.H., Ogata, Y. and Kaneko, K., 2003a, Strain rate dependency of the dynamic tensile strength of rock. Int. J. Rock. Mech. Min. Sci., Vol.40, No.5, pp. 763-777.
3) Cho, S.H., Nishi, M., Yamamoto, M. and Kaneko, K., 2003b, Fragment size distribution in blasting, Mater. Trans, Vol.44, No.5, pp.951-956.
4) Cho. S.H. and Kaneko, K., 2004, Influence of the applied pressure wave form on the dynamic fracture processes in rock, Int. J. Rock. Mech. Min. Sci., Vol. 41, pp.771-784.
5) Cho, S.H., Mohanty, B., Ito, M., Nakamiya, Y., Owada, S., Kubota, S., Ogata, Y., Tsubayama, A., Yokota, M. and Kaneko, K., 2006, Dynamic fragmentation of rock by high-voltage pulses, Int. Proceedings of 41st US symposium on rock mechanics, Curran Associates, Inc., 06-1118.
6) Cho, S.H., Nakamura, Y., Mohanty. B, Yang. H.S, Kaneko. K, 2008, Numerical study of fracture plane control in laboratory-scale blasting, Engineering Fracture mechanics, Vol. 75(13), pp.3966-3984.
7) Duvall W.I.,1953, Strain-wave shapes in rock near explosions, Geophysics, Vol.18, No.2, pp.310-323.
8) Fukuda, D., Moriya, K., Kaneko, K., Sasaki, K., Sakamoto. R, Hidani. K, 2012, Numerical simulation of the fracture process in concrete resulting from deflagration phenomena, Int. J. Fract, Vol.180, No.2, pp.163-175.
9) Ito, I., and Sassa, K., 1968, On the mechanism of breakage by smooth blasting, J. of the Mining and Metallurgical Institute of Japan 84, 964: 1059-1065 [in Japanese].
10) Kaneko, K., Matsunaga, Y. and Yamamoto, M., 1995, Fracture mechanics analysis of fragmentation process in rock blasting, Sci. Tech. Energetic Materials, Vol.56, pp.207-215 [in Japanese].

11) Nakamura, Y., Kato, M., Ogata, Y., Okina. Y, Nakamura. S, Yamamoto. M, 2009, Model experiments on fracture plane control in blasting, Japan Explosive Society, pp. 9-120 [In Japanese].

12) Sassa, K. and Ito, I., 1972, Journal of The Society of Materials Science, Vol.21, pp.123-129 [in Japanese].

CHAPTER 4

FRACTURE CONTROL IN CYLINDRICAL CONCRETE PILE BY STEEL PLATE

4.1 INTRODUCTION

The breakage of concrete pile head by conventional mechanical methods involves both the safety risks to the site workers and general public living in the vicinity and noise hazard. Thus, alternative methods have been required (Takahashi *et al*., 2006) and, for the rapid and well-controlled removal of cylindrical concrete pile head, Nakamura *et al*. (2009) proposed an application of a dynamic breakage system by blasting in which the charge holder as a controller of crack initiation direction and steel plate as a crack arrester were installed inside the cylindrical concrete pile head at the curing stage of concrete. The effectiveness of the dynamic breakage system was proved in both laboratory-scale and field-scale blast experiments (e.g., Nakamura *et al*. 2009; Kato *et al*. 2009; Cho *et al*. 2011; Nakamura *et al*. 2013). Although these experimental results were successful, it was difficult to understand the detailed mechanism of crack growth occurring inside the concrete pile and to find the optimum designs such as the best shape of the charge holder and the best installation location of crack arrester. As pointed out through the verification of DFPA-A in Chapter 3, the 3-D propagation of conical cracks from the bottom corner of the charge hole can occur and investigation of control of this crack is of significant importance in terms of the prevention of the damage in the remaining concrete pile after the removal of the pile head. However, conventional 2-D DFPA (e.g., Kaneko *et al*. 1995;

Yamamoto *et al*. 1999; Cho 2003; Cho *et al*. 2003a, b; Cho and Kaneko 2004; Cho *et al*. 2006, 2008; Fukuda *et al*. 2013) cannot analyze this problem and thus DFPA-A proposed and developed in Chapters 2 and 3 can be applicable for the investigation of the effectiveness of crack arrester in the dynamic breakage system for the removal of cylindrical concrete pile head.

In this chapter, the dynamic breakage system for the removal of a cylindrical concrete pile head by blasting with the hollow steel plate proposed by Nakamura *et al*. (2009) is experimentally and numerically investigated. First, to prove the effectiveness of hollow steel plate as a crack arrester for the purpose of minimization of the damages in the remaining part of concrete pile, two types of experiments and DFPA-A with/without the application of the steel plate are conducted and the applicability of the steel plate is shown. Then, assuming the laboratory-scale experiment of concrete pile head removal by blasting a cylindrical charge with a hollow steel plate, DFPA-A is conducted to investigate the influence of both the loading rate and spacing between steel plate and charge hole on the resultant fracture pattern, and the obtained fracture patterns are compared.

4.2 EXPERIMENT

4.2.1 Experimental setup

In order to understand the applicability of the hollow steel plate in the dynamic breakage system for the removal of a cylindrical concrete pile head by blasting proposed by Nakamura *et al*. (2009), a laboratory-scale experiment is conducted. Figure 4.1 shows the information of the specimen used in the experiment. A cylindrical concrete pile with both the diameter and height of 600 mm is prepared in which both the octagon shaped charge holder and hollow plate made of galvanized steel are installed. The inner and outer diameters of the hollow steel plate are 250 mm and 510 mm, respectively, and its thickness is 1.5 mm. The fixer made of steel is also used for the purpose of the reduction of shock wave generated from charge

holder. For charge conditions, the seismic electronic detonator (No.8) (Stark, 2010) and an explosive called “New Fineker” made by Hanwha cooperation, South Korea (Lee *et al*. 2001), are used as shown in Fig. 4.2. Average detonation velocity and bulk density of the New Fineker are 3400 m/s and 0.82 g/cc, respectively. The charge weight, diameter and length of the New Fineker used in this experiment are 13 g, 35 mm and 100 mm, respectively. Then, the space above the New Fineker in the charge holder was filled by the tamping material, i.e. rapidly curing cement. The volumes of the charge holder except tamping material (V_c) and explosive (V_e) are 198.17 cm^3 and 96.21 cm^3, respectively. Therefore, the volumetric decoupling ratio (Rustan, 1998) defined by V_c / V_e is 2.06, resulting in relatively slower rise time of the generated pressure. The uniaxial compressive strength of concrete is 41 MPa. Then, the resultant fracturing pattern is observed. For the comparison, the fracturing pattern in the concrete specimen without the application of the hollow steel plate is also conducted.

4.2.2 Experimental results

Figs. 4.3 and 4.4 show the fracture patterns obtained from the experiments in Fig. 4.1 for the cases with/without the application of the steel plate, respectively. As is evident from Fig. 4.3, the case without the steel plate results in the crack propagation to the bottom part of concrete, i.e. the damage in the remaining part of concrete pile. On the other hand, the case with the steel plate results in well-controlled crack pattern, i.e. no crack toward the bottom part of concrete pile. In addition, the upper part of the specimen in both cases, i.e. concrete pile head, is split into two pieces because the charge holder has the two slits at the opposite sides where the large stress concentration due to the application of detonation pressure occurs. From these results, the effectiveness of steel plate on controlling fractures and minimizing the damages of remaining part of the concrete pile is indicated. However, with only these experiments, the identification of ideal type of explosive, i.e. characteristics of applied pressure wave form, and

installation location of the steel plate to minimize the damage to the remaining concrete pile is difficult to investigate.

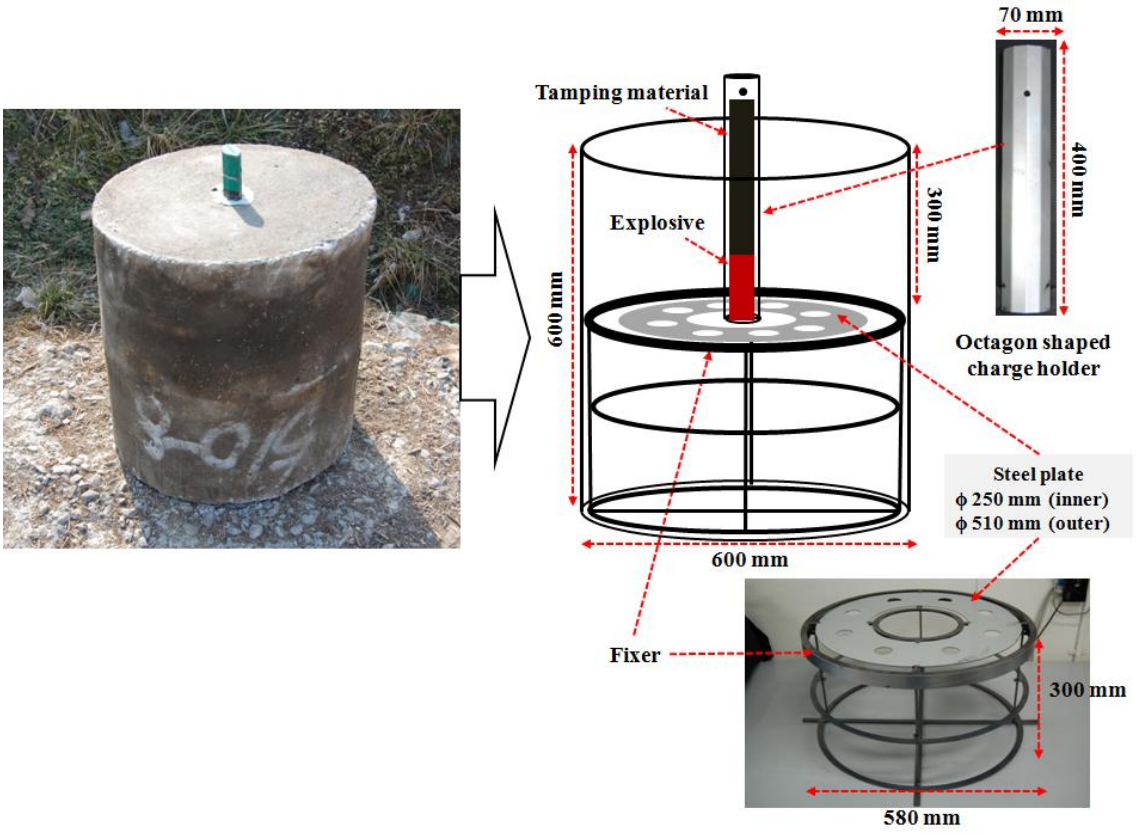

Figure 4.1 Description of the specimen in laboratory-scale experiment.

Figure 4.2 New fineker explosive used in laboratory-scale experiment.

Figure 4.3 Result of blasting experiment without the steel plate

Figure 4.4 Result of blasting experiment with the steel plate

4.3 NUMERICAL SIMULATION

4.3.1 Model description

To simulate the dynamic fracturing process in cylindrical concrete pile, the DFPA-A assuming the same experimental configuration as in Fig. 4.1 is conducted and the fracture mechanism is numerically investigated in detail. In Fig. 4.5, a model of cylindrical concrete pile

with a cylindrical charge hole and hollow steel plate is shown with the size information and corresponding FEM mesh. Because the effectiveness of the shaped charge holder is independently discussed in Chapter 5, and the cylindrical charge hole without steel wall is assumed in this chapter. In the mesh generation, the size of each 3-node triangular ring element is set to be small enough to avoid the mesh dependency of crack path. The analysis model has three free faces on the upper, lateral and bottom part of model. The total number of elements and initial nodes are 79247 and 40000, respectively. The physical properties of the concrete and steel plate which are experimentally determined are listed in Table 1. As is evident from the table, it is assumed that the no fracturing occur in the steel plate which is justified from the experimental result in Figs. 4.3 and 4.4. In addition, the physical properties of tamping material are assumed to be same as concrete and its strength is set large enough not to allow the crack propagation into the tamping material. The strength on the boundary between the steel plate and concrete is expressed by that of concrete. For the applied pressure $P(t)$ at time t, the following equation is used to investigate the influence of both maximum pressure and rise time on the fracture pattern (Duvall 1953; Ito 1968):

$$P(t) = P_0 \xi \{\exp(-\alpha t) - \exp(-\beta t)\} \tag{4.1}$$

$$\xi = 1/\{\exp(-\alpha t_0) - \exp(-\beta t_0)\} \tag{4.2}$$

where α and β are constants, ξ, normalization constant, P_0, maximum pressure and t_0, rise time of the pressure. P_0 =100 MPa is used for all analyses in this chapter. The t_0 is given in the following form:

$$t_0 = \{1/(\beta - \alpha)\} \log(\beta / \alpha)\} \tag{4.3}$$

where β/α = 1.5 is used for all analyses in this chapter.

In the following, the DFPA-As with/without the application of the steel plate are conducted. Then, the influence of both t_0 and the distance between charge hole and steel plate, S_b, on the resultant fracture pattern, and the obtained fracture patterns are compared for each case in Table 4.2. Figure 4.6 shows the pressure-time curve for applied pressure waveforms in each case in Table 4.2.

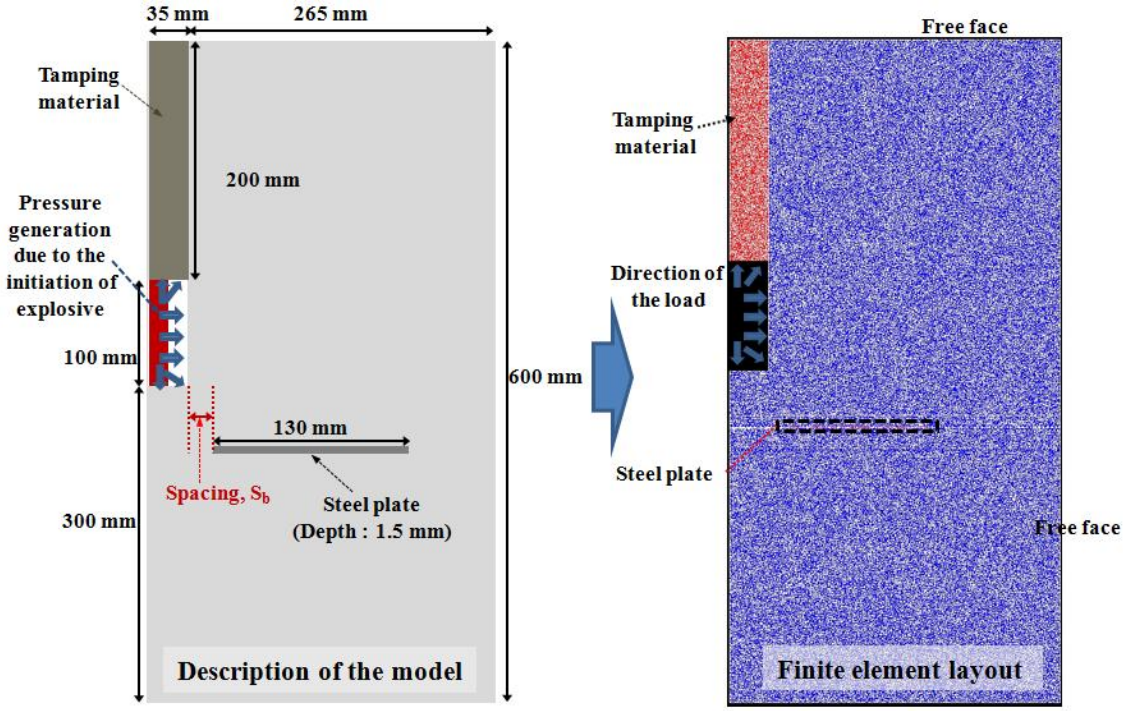

Figure 4.5 Description of the finite element mesh having a hollow steel plate

Table 4.1. Physical properties of concrete.

Materials	Parameters	Value
Concrete	Density, ρ (kg/m^3)	2170
	Elastic modulus, E (GPa)	36.17
	Poisson's ratio, v (--)	0.25
	Mean tensile strength, S_t (MPa)	4
	P wave velocity, V_p (m/s)	4500
	S wave velocity, V_s (m/s)	2601
	Coefficient of uniformity, m (--)	5
Steel plate	Density, ρ (kg/m^3)	7900
	Elastic modulus, E (GPa)	207
	Poisson's ratio, v (--)	0.33
	Mean tensile strength, S_t (MPa)	290
	P wave velocity, V_p (m/s)	6100
	S wave velocity, V_s (m/s)	3500

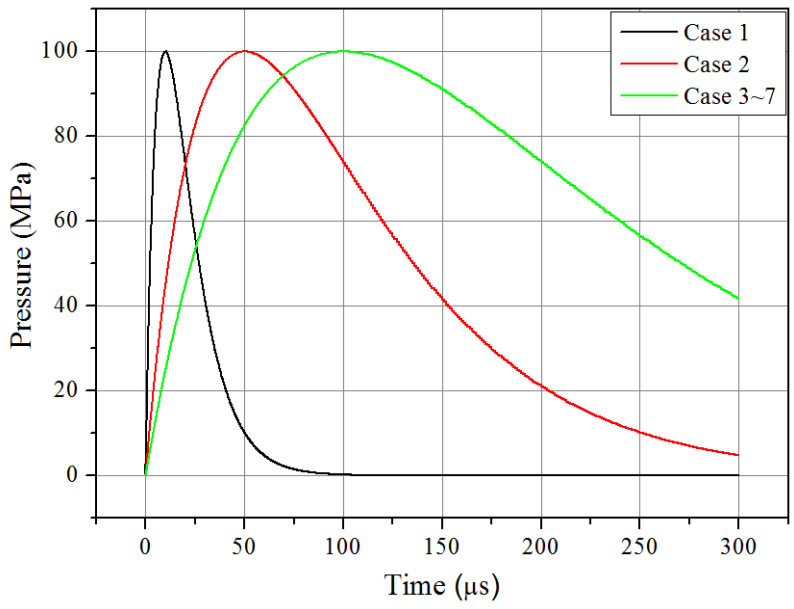

Figure 4.6 Pressure-time curves for each case in Table 4.2.

Table 4.2. Conditions of the analysis models.

Case	Maximum pressure, P_0 (MPa)	Rise time, t_0 (μs)	Spacing between steel plate and charge hole, S_b (mm)
1	100	10	90
2	100	50	90
3	100	100	90
4	100	50	5
5	100	50	15
6	100	50	35
7	100	50	65

4.3.2 Fracture pattern in the cases with/without steel plate

In Fig. 4.7, the result of DFPA-A, i.e. the progress of tensile fracturing without the steel plate, is shown from t = 0 to 150 μs. The result corresponding to Case 3 is chosen considering the volumetric decoupling ratio and S_b used in the experiment. In the figure, the tensile fracturing occurring in both r-z and r-θ planes (hereafter, r-z and r-θ tensile fractures, respectively) introduced in Chapter 2 are expressed in solid black lines and red regions, respectively. The r-z and r-θ tensile fractures include the fracture process zone and opened fracture. These rules are also applied in the presentation of following figures in this chapter. Around 15 μs, it is observed that both the r-z and r-θ tensile fractures are initiated from the side wall of the charge hole. Then, at t = 30 μs,the predominant r-z tensile fractures extending obliquely upward and downward from the top and bottom corners of the charge hole, respectively, are found. The mechanism of the occurrence of these predominant fractures, i.e.

conical cracks, was already discussed in Chapter 3. Then, between t = 30 ~ 105 μs, these conical cracks continued extending. In addition, r-θ tensile fractures mainly occur in the way that the conical cracks surround the r-θ tensile fractures for these time intervals. It is also noted that, after around t =105 μs, both the initiation and downward propagation of the conical cracks and r-θ fractures are also found from top outer boundary of concrete pile. At around t = 150 μs, the r-θ tensile fractures almost reach at the lateral outer free face of the model, resulting in splitting the specimen by r-θ tensile fracture as well as the occurance of two predominant conical cracks form the top and bottom corners of charge hole.

On the other hand, Fig. 4.8 shows the result of DFPA-A with the steel plate in Case 3 from t = 0 to 150 μs. Similar to the case without the steel plate, at around t = 15 μs, the predominant conical cracks from the bottom and top corners of the charge hole are found. The conical crack extending upward shows the smilar propagation manner as in Fig. 4.7 because no crack arrester is used in this direction. However, the conical crack extending downward starts interacting with the steel plate at around t = 45 μs. Then, although the minor extension of the conical crack below the steel plate is still observed, the resultant length of this conical crack is clearly reduced by the existence of the steel plate. In addition, comparing the r-θ tensile fracturing in the cases with/without the steel plate, the r-θ tensile fractures with the steel plate cleary results in the less fracturing below the steel plate and the effectiveness of steel plate to reduce the damage in the remaining part of concrete pile is now justified.

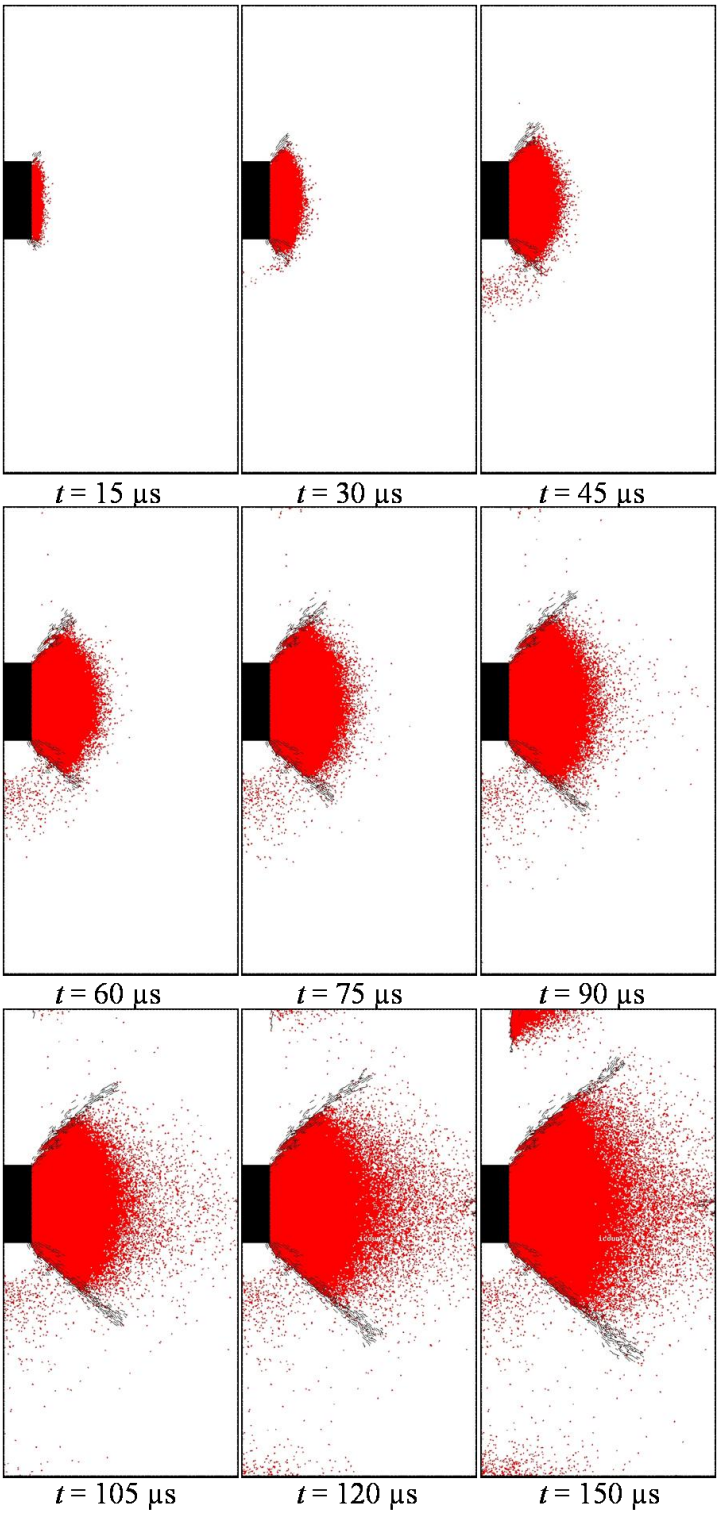

Figure 4.7 Result of fracture process without the steel plate in Case 3

(P_0 = 100 MPa, t_0 = 50 μs).

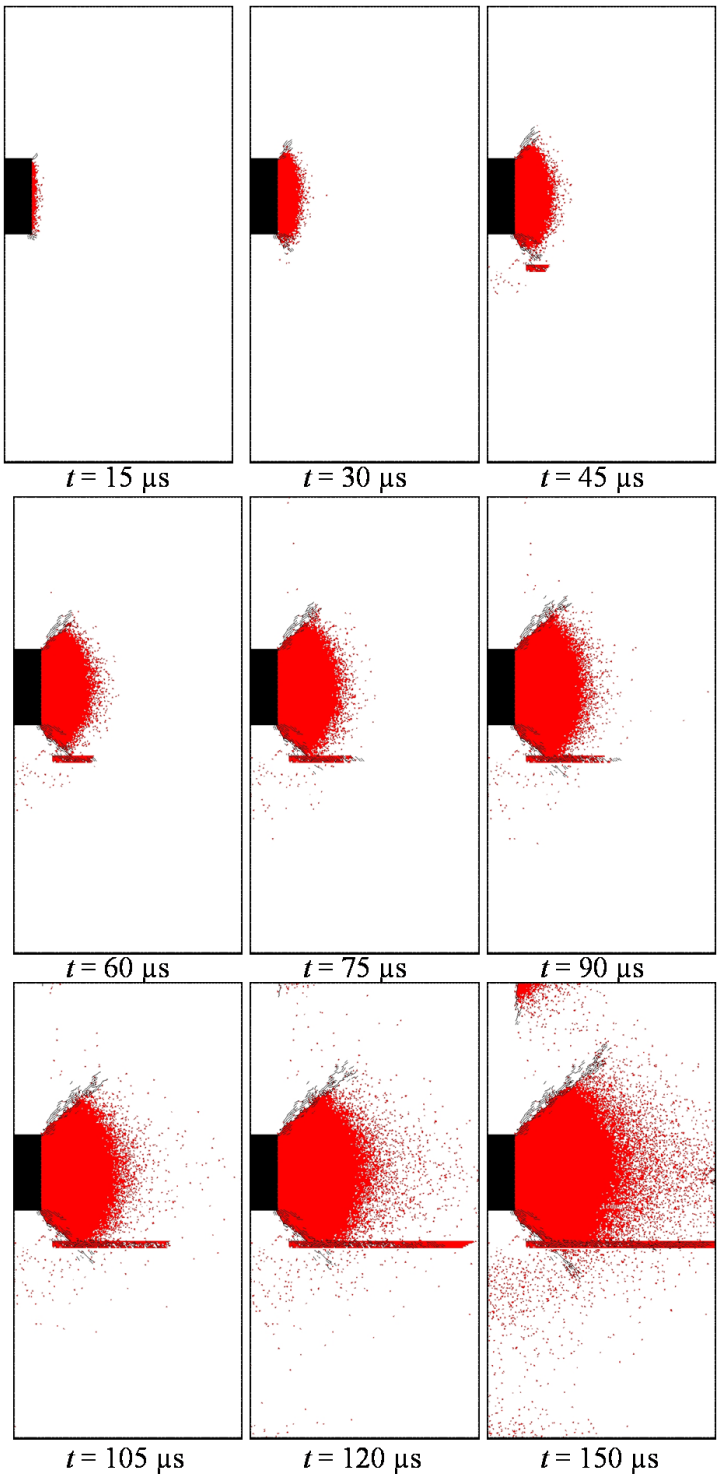

Figure 4.8 Result of fracture process in Case 3

(P_0 = 100 MPa, t_0 = 50 μs, S_b = 90 mm)

4.4 DISCUSSION

4.4.1 Influence of applied pressure on fracture pattern

To examine the influence of loading rate on the resultant of fracture pattern, the results of DFPA-A for Cases 1, 2 and 3 in Table 4.2 are compared, in which all the cases use the same values of P_0 and S_b but different t_0. Figure 4.9 shows comparison of the resultant fracture patterns for Cases 1, 2 and 3 at t = 150 μs. All of these results show that the predominant r-θ tensile fractures occur from the lateral wall of charge hole which are bounded by predominant r-z tensile fractures, i.e. conical cracks initiated from the bottom and top corners of charge hole. The fracturing occurring above the steel plate is more or less similar to each other with minor differences around the top free face.

By comparing these three cases in terms of the degree of damage in the remaining part of concrete pile below the steel plate, Case 1 with the shortest rise time results in the worst fracture pattern in which the intense r-θ and r-z tensile fractures occur just below the bottom of charge hole although the r-θ tensile fractures and conical crack from the bottom corner of charge hole is not significant below the steel plate. On the other hand, Case 3 with the longest rise time results in the shortest conical crack and least r-θ tensile fractures occurring below the steel plate. Case 2 also shows the similar result to that of Case 3 with slightly longer conical crack and slightly more intense r-θ tensile fractures below the steel plate.

Therefore, in case that the t_0 is considered as variable, blasting conditions with the larger t_0 than 50 μs is more effective for arresting the conical crack propagation and to preventing the damages in the remaining part of concrete pile below the steel plate. In addition, it is also indicated that larger t_0 can results in less r-θ tensile fractures below the steel plate.

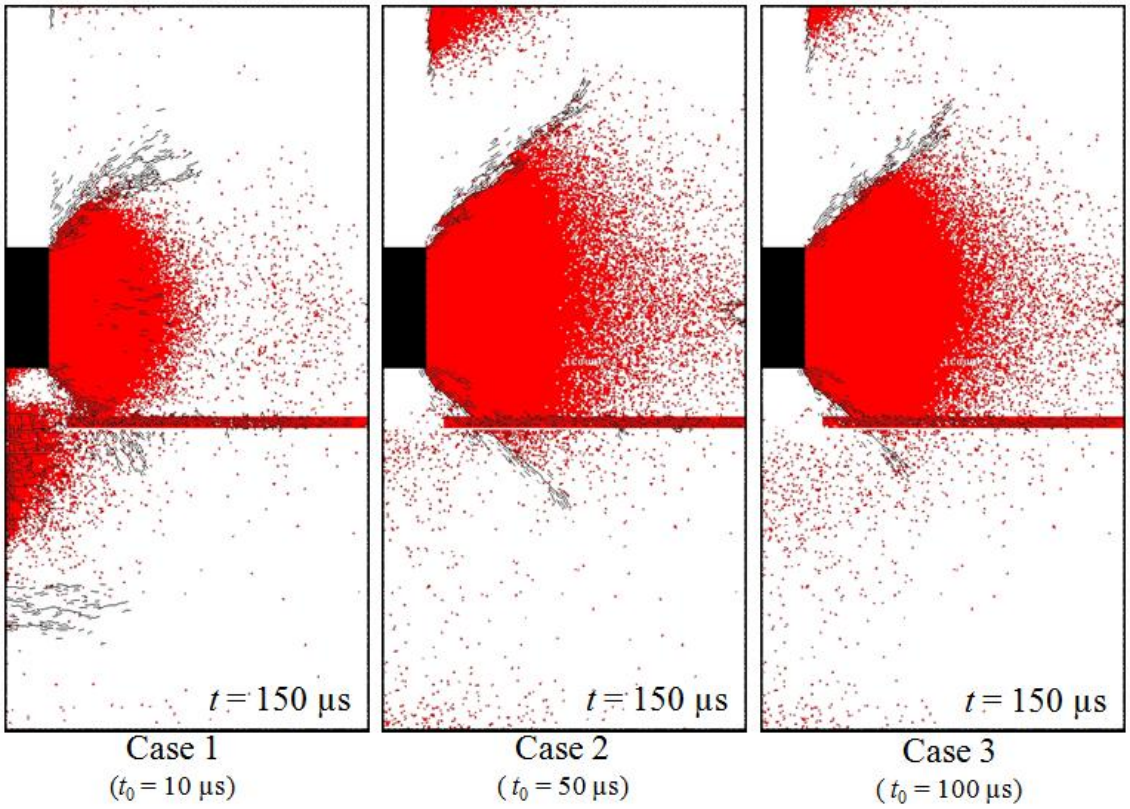

Figure 4.9 Influence of rise time, t_0, on the resultant fracture pattern (P_0 = 100 MPa, S_b = 90mm).

4.4.2 Influence of spacing between steel plate and charge hole on fracture pattern

To examine the influence of S_b on the resultant fracture pattern, the DFPA-A for Cases 4, 5, 6 and 7 in Table 4.2 are compared, in which all the cases use the same values of P_0 and t_0 but different S_b. Figure 4.10 shows the comparison of the resultant fracture patterns for Cases 4, 5, 6 and 7 at t = 150 μs. All of these results show that the predominant r-θ occur from the lateral wall of charge hole which are bounded by predominant r-z tensile fractures, i.e. conical cracks initiated from the bottom and top corners of charge hole. The fracturing occurring above the steel plate is quite similar to each other with minor differences around the top free face.

By comparing the four cases in terms of the degree of damage in the remaining part of concrete pile below the steel plate, Case 4 with the shortest S_b results in the best fracture pattern in which little conical crack and r-θ tensile fractures occur below the steel plate. On the other hand, Cases 5, 6 and 7 with relatively larger S_b result in longer conical crack and more or less r-θ tensile fractures occurring below the steel plate because the interaction of crack propagation from the charge hole with the steel plate is compromised in these cases.

Therefore, in case that the S_b is considered as variable, blasting conditions with the installation distance of the hollow steel plate less than 5 mm from charge hole is more effective for arresting the conical crack propagation to the remaining part of concrete pile below the steel plate. In addition, it is also indicated that smaller S_b can also result in less r-θ tensile fractures below the steel plate.

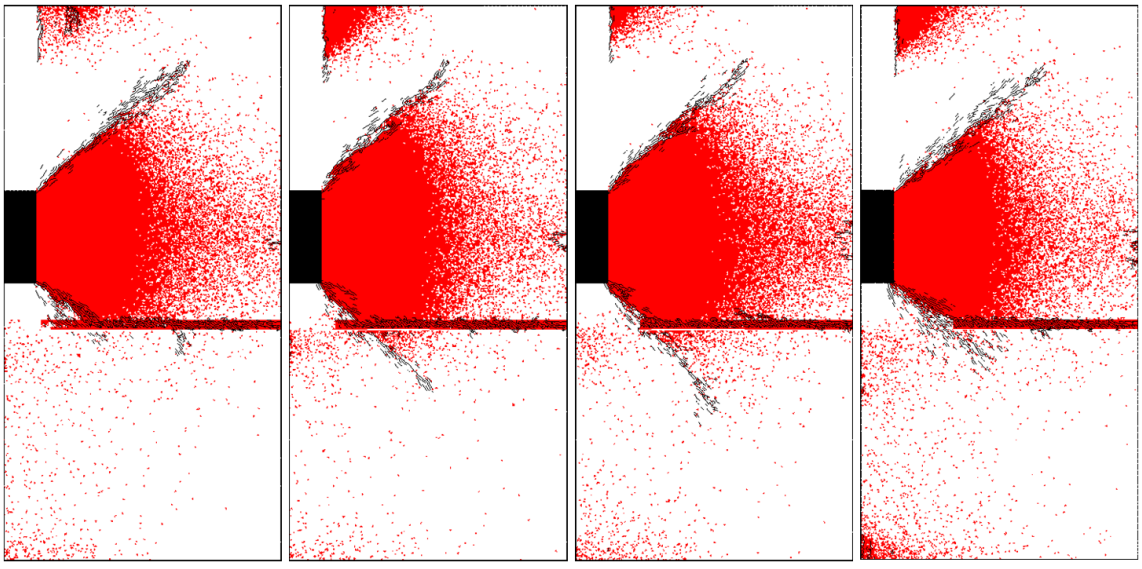

Figure 4.11 Influence of spacing between steel plate and charge hole, S_b, on fracture pattern (P_0 = 100 MPa, t_0 = 50 μs).

4.5 CONCLUDING REMARKS

In this chapter, a dynamic breakage system by blasting with a hollow steel plate as a crack arrester proposed by Nakamura *et al*. (2009) for the removal of a cylindrical concrete pile head was experimentally and numerically investigated.

First, to prove the effectiveness of hollow steel plate as a crack arrester for the purpose of minimization of the damages in the remaining part of concrete pile, two types of experiments and DFPA-As with/without the application of the steel plate were conducted. The experimental and numerical results clearly showed that the case with the steel plate resulted in better fracture pattern in which the damage in the remaining concrete pile below the steel was reduced, while the case without the steel plate resulted in significant fracturing toward remaining part of concrete pile.

Then, to investigate the influence of both the loading rate characterized by rise time t_0 of the applied pressure and spacing between steel plate and charge hole, S_b, on the resultant fracture pattern, various DFPA-As assuming the laboratory-scale experiment of concrete pile head by blasting a cylindrical charge with a hollow steel plate was conducted and the obtained fracture patterns were compared in terms of the minimization of the damage in the remaining part of the concrete pile owing to the dynamic removal of concrete pile head.

In case that the t_0 is considered as variable, blasting conditions with the larger t_0 than 50 μs was found to be more effective for arresting the conical crack propagation and prevention of the damages in the remaining part of concrete pile below the steel plate. In addition, it was indicated that the larger t_0 could result in less r-θ tensile fractures below the steel plate. On the other hand, in case that the S_b was considered as variable, blasting conditions with the installation distance of the hollow steel plate less than 5 mm from charge hole was found to be more effective for arresting the conical crack propagation to the remaining part of concrete pile below the steel plate. Therefore, considering all the DFPA-A results, the application of loading

condition which realizes the relatively slower loading rate, i.e. $t_0 > 50$ μs, and $S_b < 5$ mm should be used to obtain the optimized fracture pattern.

BIBLIOGRAPHY

13) Cho, S.H., 2003, Dynamic fracture process analysis of rock and its application to fragmentation control in blasting, Doctor dissertation, Hokkaido University, Japan.

14) Cho, S.H., Ogata, Y. and Kaneko, K., 2003a, Strain rate dependency of the dynamic tensile strength of rock. Int. J. Rock. Mech. Min. Sci., Vol.40, No.5, pp. 763-777.

15) Cho, S.H., Nishi, M., Yamamoto, M. and Kaneko, K., 2003b, Fragment size distribution in blasting, Mater. Trans, Vol.44, No.5, pp.951-956.

16) Cho. S.H. and Kaneko, K., 2004, Influence of the applied pressure wave form on the dynamic fracture processes in rock, Int. J. Rock Mech.Min. Sci., Vol.41, pp.771-784.

17) Cho, S.H., Mohanty. B., Ito, M., Nakamiya, Y., Owada, S., Kubota, S., Ogata, Y., Tsubayama, A., Yokota, M. and Kaneko, K., 2006, Dynamic fragmentation of rock by high-voltage pulses, Int. Proceedings of 41st US symposium on rock mechanics, Curran Associates, Inc., 06-1118.

18) Cho, S.H., Nakamura, Y., Mohanty. B, Yang. H.S, Kaneko. K, 2008, Numerical study of fracture plane control in laboratory-scale blasting, Engineering Fracture mechanics, Vol. 75(13), pp.3966-3984.

19) Cho. S.H, Ahn. J.L, Kim. S.G, Park. H, Ko. J.H and Suk. C.G, 2011, Effectiveness of simplified charge holder on the crack propagation control in blasting, The 6th International Conference on Explosives and Blasting, pp.132-134.

20) Duvall W.I.,1953, Strain-wave shapes in rock near explosions, Geophysics, Vol.18, No.2, pp.310-323.

21) Fukuda, D., Moriya, K., Kaneko, K., Sasaki, K., Sakamoto. R, Hidani. K, 2012, Numerical simulation of the fracture process in concrete resulting from deflagration phenomena, Int. J. Fract, Vol.180, No.2, pp.163-175.

22) Ito, I., and Sassa, K., 1968, On the mechanism of breakage by smooth blasting, J. of the Mining and Metallurgical Institute of Japan 84, 964: 1059-1065 [in Japanese].

23) Kaneko, K., Matsunaga, Y. and Yamamoto, M., 1995, Fracture mechanics analysis of fragmentation process in rock blasting, Sci. Tech. Energetic Materials, Vol.56, pp.207-215 [in Japanese].

24) Kato M, Nakamura Y, Ogata Y, Kubota S, Matsuzawa T, Nakamura S, Adachi T, Yamaura I, Yamamoto M, 2009, Research on the dynamic fragment control of pile head using a charge holder, Japan Explosive Society, Vol. 70, pp. 108-111. (In Japanese).

25) Lee, C.S., Lee, Y.J., Kim, H.S., Song, Y.S. and Kwon, O.S., 2001, Practical use of blast pattern utilizing new finecker, Journal of Korean society of explosives and blasting, Vol.19, pp.27-37 [in Korean].

26) Nakamura, Y., Kato, M., Ogata, Y., Okina. Y, Nakamura. S, Yamamoto. M, 2009, Model experiments on fracture plane control in blasting, Japan Explosive Society, pp. 9-120 [In Japanese].

27) Nakamura. S, Takeuchi. H, Nakamura. Y, Higuchi. T, 2013, Development of the dynamic removal method for concrete pile head using charge holder producing horizontal fracture plane, the 7th international conference on explosives and blasting in China, pp. 197-208.

28) Rustan, A., 1998, Rock Blasting Terms and Symbols: A Dictionary of Symbols and Terms in Rock Blasting and Related Areas like Drilling, Mining and Rock Mechanics.

29) Stark, A., 2010, Seismic methods & applications: A guide for the detection of geologic structures, Earthquake zones and hazards, resources exploration and geotechnical engineering, BrownWalker Press.

30) Takatoshi, I., Masanori. M., Mitsuru. S., 2006, Development of removed pile method with cutting, Preceedings of the world tunnel congress and 32nd ITA Aseembly, pp.22-27.

31) Yamamoto, M., Ichijo, T., Inaba, T., Morooka, K., and Kaneko, K., 1999, Experimental and theoretical study on smooth blasting with electronic delay detonators, Int. J. of Rock Fragmentation by Blasting, Vol.3, No.1, pp.3-24.

CHAPTER 5

FRACTURE CONTROL IN CONCRETE PILE BY CHARGE HOLDER

5.1 INTRODUCTION

As mentioned in previous chapters, the application of blasting for the quick removal of concrete pile head has been proposed by Nakamura *et al*. (2009) which utilized both the shaped charge holder and hollow steel plate installed inside the concrete pile head at the curing stage of concrete. The effectiveness of the steel plate as a crack arrester was investigated and the optimum design for the well-controlled breakage was discussed in Chapter 4. For the effectiveness of the charge holder as a direction controller of crack initiation and propagation, Nakamura *et al*. (2010) applied the wedged charge holders to the dynamic breakage and suggested the angle of 30° of wedged charge holder for controlling crack initiation direction inside the rectangular concrete structure. Although their blasting experiment proved the effectiveness of charge holders to control the crack propagation under particular condition, the optimum loading conditions for the well-controlled breakage of concrete pile was not clarified. As pointed out in Chapter 2, to simulate the fracturing process in the huge concrete pile with rectangular cross section occurring over multiple charge holders, the DFPA-A proposed and developed in this dissertation cannot be applied and thus the DFPA for 2-D plane strain problem can instead be useful considering its performance and applicability to various dynamic fracturing problems (e.g., Kaneko *et al*. 1995; Yamamoto *et al*. 1999; Cho 2003; Cho *et al*. 2003a,b; Cho and Kaneko 2004; Cho *et al*. 2006, 2008; Fukuda *et al*. 2013).

In this chapter, the dynamic breakage of concrete pile head with the application of with the wedged charge holders proposed by Nakamura (2010) is investigated in detail. For this purpose, the result of field-scale experiment by Nakamura (2010) is first introduced and reviewed. Then, assuming the experimental setting in Nakamura (2010), the fracturing process is investigated by the DFPA for 2-D plane strain problem in which the influence of various loading conditions on the resultant fracture patterns as well as the optimum design to achieve the controlled fracturing are discussed by clarifying the mechanism of dynamic fracture processes particular to this problem.

5.2 EXPERIMENT

5.2.1 Experiment setup

Figure 5.1 (a) shows the size of rectangular shaped concrete pile and alignment of charge holders corresponding to the experiment in Nakamura (2010). The purpose of the experiment was to induce the fracturing along the expected fracture planes and to reduce the damage in the remaining area. The four wedged charge holders in total were installed in the concrete specimen at the curing stage. The width, length and depth of concrete specimen were 1500 mm, 2000 mm and 1000 mm, respectively. Fig. 5.1 (b) shows the shape and size of each wedged charge holder for one of two sides with its 3D configuration shown in Fig. 5.1 (c). The charge holder was made of galvanized steel. The angles of each corner, θ_1 and θ_2, of the charge holder were 30^o and 120^o, respectively. The width, length and thickness of the charge holder were 80 mm, 46 mm and 1.6 mm, respectively. For the charge condition of each charge holder, the seismic electronic detonator (No.6) (Stark, 2010) and an explosive called “CCR (Japanese explosive industry, 2002)” made by Kayaku Japan, Co., Ltd., Japan, were used. Mean combustion rate and gas volume of the CCR were 40 ~ 60 m/s and 160 ~ 180 cm^3/g, respectively, with the charge weight of 57 g used in this experiment.

Figure 5.2 shows the photo of breakage of concrete specimen after the experiment. The result shows that quite smooth fracture plane was obtained along the expected fracture plane and little damage was observed toward the remaining part of the specimen. Thus, under this condition, the applicability of the shaped charge holders is verified. However, the mechanism of the controllability of crack initiation and propagation directions cannot be understood well only from this experiment.

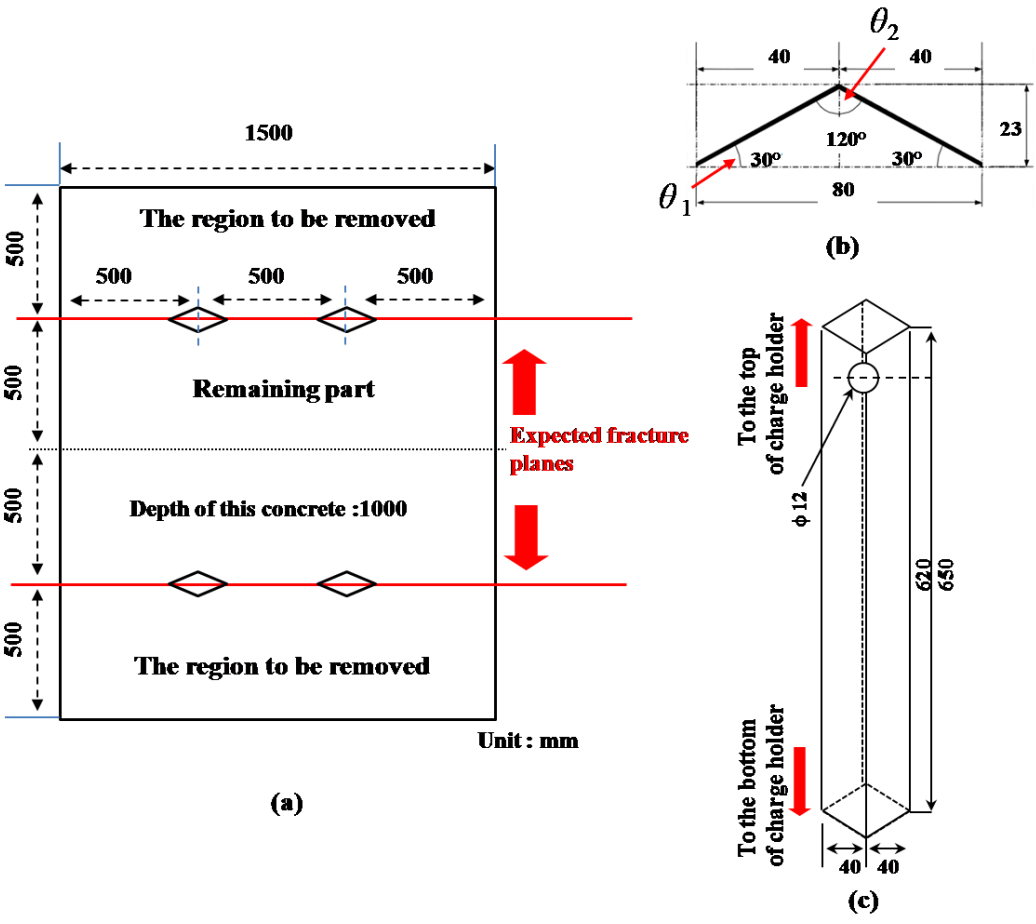

Figure 5.1 Alignment of charge holder in concrete specimen and shape of wedged charge holder by Nakamura *et al*., 2010 (unit: mm).

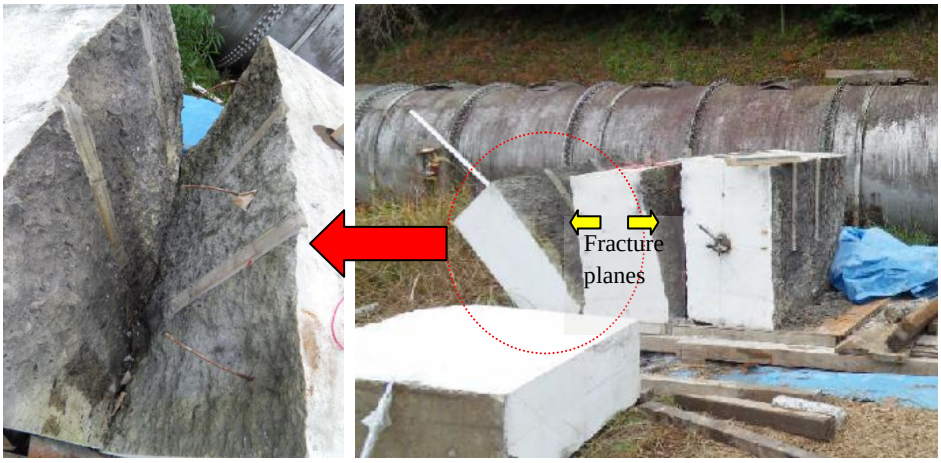

Figure 5.2 Resultant facture plane after blasting experiment by Nakamura *et al*. (2010).

5.3. NUMERICAL RESULTS

5.3.1 Model description

Assuming the experimental configuration in Nakamura *et al.* (2010), the DFPA for 2-D plane strain problem is applied and fracturing mechanism is numerically investigated in detail. In Fig. 5.3, a model of rectangular concrete pile with the two wedged charge holders is shown with the size information and corresponding FEM mesh discretized by 3-node triangular elements. The perimeter boundaries of the model are treated as free faces. The minimum size of the elements used in this study is approximately 1 mm. The total number of elements and initial nodes are 119132 and 60000, respectively. In Table 5.1, the physical properties of concrete and charge holder used for the DFPA are listed. The charge holder is assumed to be homogeneous and thus constant tensile strength is used. In addition, although the DFPA code for 2-D plane strain problem supports the treatment of compressive fracture, only the tensile fracturing is taken into account considering the fact that little yielding in the steel and crushing in the concrete was observed in the above experiment and tensile fracturing dominates in this class of problem. For the applied pressure $P(t)$ at time t, the following equation is used to investigate the

influence of both maximum pressure and rise time on the resultant fracture pattern (Duvall 1953; Ito 1968):

$$P(t) = P_0 \xi \{\exp(-\alpha t) - \exp(-\beta t)\} \tag{5.1}$$

$$\xi = 1/\{\exp(-\alpha t_0) - \exp(-\beta t_0)\} \tag{5.2}$$

where α and β are constants, ξ, normalization constant, P_0, maximum pressure and t_0, rise time of the pressure. The expression of t_0 is given as follows:

$$t_0 = \{1/(\beta - \alpha)\}\log(\beta/\alpha)\} \tag{5.3}$$

where β/α = 1.5 is used for all the analyses in this chapter.

To investigate the influence of loading condition on the corresponding dynamic fracture processes and resultant fracture patterns, the various values of P_0 and t_0 are considered as shown in Table 5.2, and Fig. 5.4 shows the pressure-time curves for the applied pressure waveforms in each case in the table.

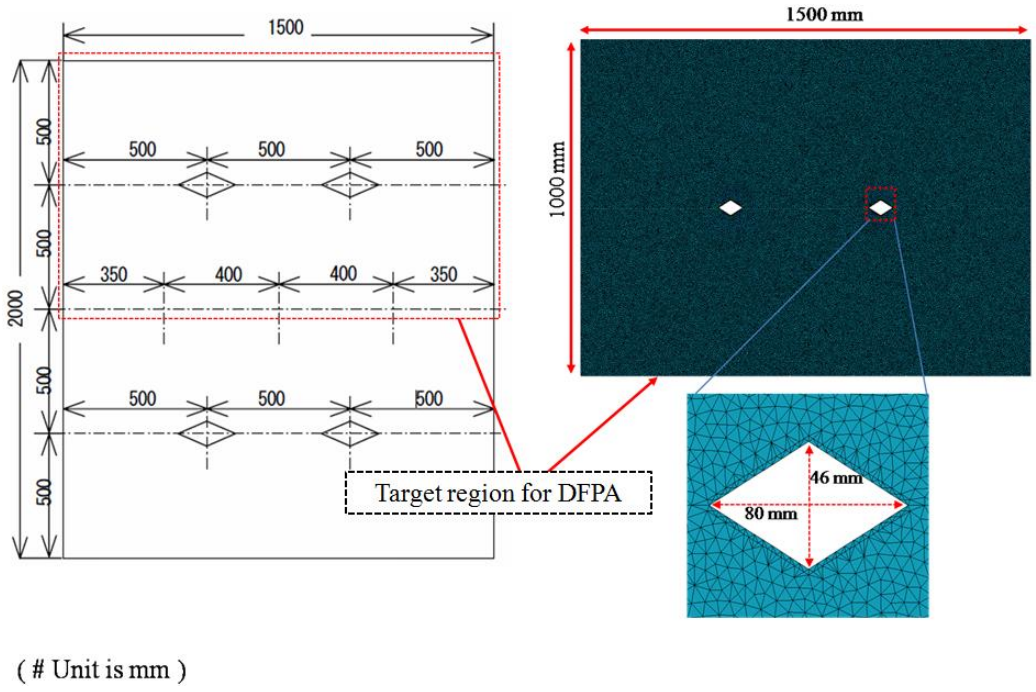

Figure 5.3 Description of the finite element mesh with charge holders.

Table 5.1. Physical properties of concrete and charge holder

Materials	Parameters	Value
Concrete	Density, ρ (kg/m^3)	2170
	Elastic modulus, E (GPa)	36.17
	Poisson's ratio, v (--)	0.25
	Mean tensile strength, S_t (MPa)	4
	P wave velocity, V_p (m/s)	4500
	S wave velocity, V_s (m/s)	2601
	Coefficient of uniformity, m (--)	5
Charge holder (steel)	Density, ρ (kg/m^3)	7900
	Elastic modulus, E (GPa)	207
	Poisson's ratio, v (--)	0.33
	Mean tensile strength, S_t (MPa)	290
	P wave velocity, V_p (m/s)	6100
	S wave velocity, V_s (m/s)	3500

Table 5.2 Conditions of the applied pressure

Case	Maximum pressure, P_0 (MPa)	Rise time, t_0 (μs)
1	50	50
2	50	100
3	50	150
4	100	100
5	150	100

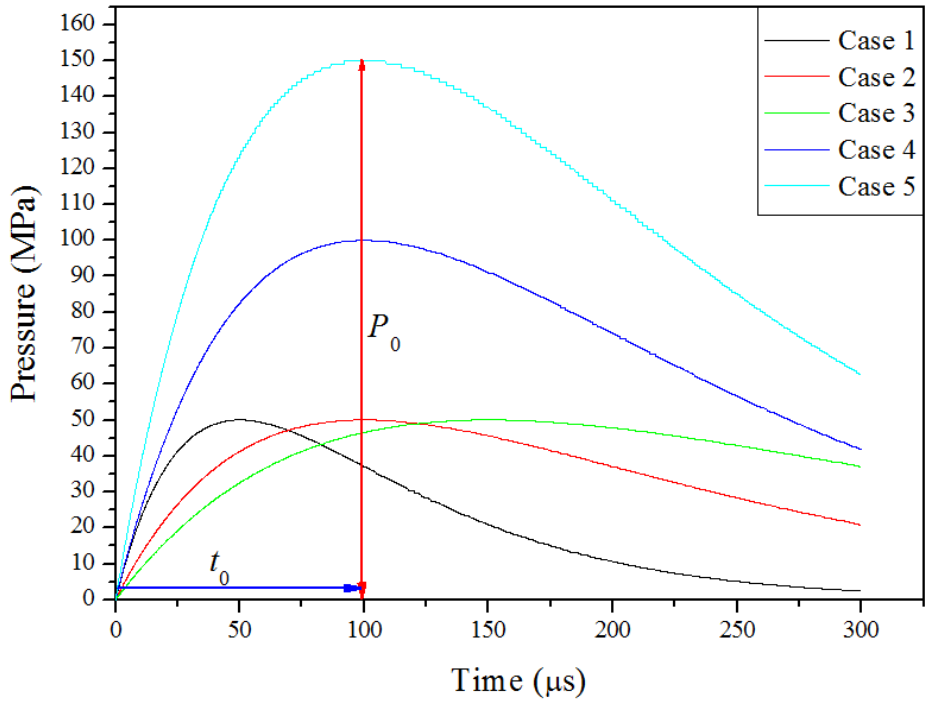

Figure 5.4 Pressure-time curves for applied pressure waveform for each case in Table 5.2.

5.3.2 DFPA results

As one of the best results in terms of the control of crack initiation and propagation directions by the charge holder, the DFPA result of Case 3 is shown in Fig. 5.5 from t = 0 to 200 μs. The figure shows the maximum principal stress distribution and crack propagation. The cold and warm colors show compressive and tensile stresses, respectively. The black lines changing with elapsed time indicate cracks initiated by the applied pressure, $P(t)$. The t = 0 corresponds to the commencement of application of pressure. At around 10 μs, tensile stress concentration is found in all the corners of each charge holder. However, because only the left and right corners of each charge holder are separated, only the leftward and rightward crack initiations occur. Then, up to t = 100 μs, it is found that the almost straight crack propagations occur and continued between each charge holder and toward lateral boundaries, respectively. However,

around t = 120 μs, because of the interaction of the stress waves from each charge holder in the center region, the crack branching occurs and coalescence of these branched cracks is found around t = 150 μs. For the cracks propagating toward lateral boundaries from each charge holder, these cracks continue to propagate in almost straight manner until they reach the outer boundaries. As a result, the cracks along the charge holders split the concrete specimen into two halves around t = 200 μs. Therefore, in this condition, the DFPA result shows the effectiveness of the application of the wedged charge holders to achieve the well-controlled splitting along expected fracture plane.

On the other hand, as one of the worst results in terms of the control of crack initiation and propagation directions by the charge holder, the DFPA result of Case 5 is shown in Fig. 5.6 from t = 0 to 200 μs, in which the main difference from Case 3 is the larger value of P_0. Similar to Case 3, tensile stress concentration is found in all the corners of each charge hole and leftward and rightward crack initiations occur up to around t = 10 μs because the left and right corners of the each charge holder are only separated. However, contrary to Case 3, the significant crack branching, i.e. unstable crack propagations occur around t = 40 μs between each charge holder and toward lateral boundaries, respectively. Then, the branched cracks between each charge holder continue to propagate and coalesce with each other around t = 80 μs in the center region. At the same time, the branched cracks toward lateral boundaries from each charge hole continue to propagate up to t = 150 μs and stopped their propagations when they reach at the outer boundaries. In addition, the initiations and propagations of predominant cracks from top and bottom boundaries toward the charge holders are found in this case, which is not significant in Case 3. As a result, the cracks along the charge holes break the concrete specimen into multiple pieces around t = 200 μs and, thus, the resultant fracture pattern is far from the achievement of well-controlled splitting along the expected fracture plane. Therefore, the obtained result indicates that the application of unnecessarily large applied pressure results in the undesirable fracture pattern in terms of the controlled breakage of concrete pile head.

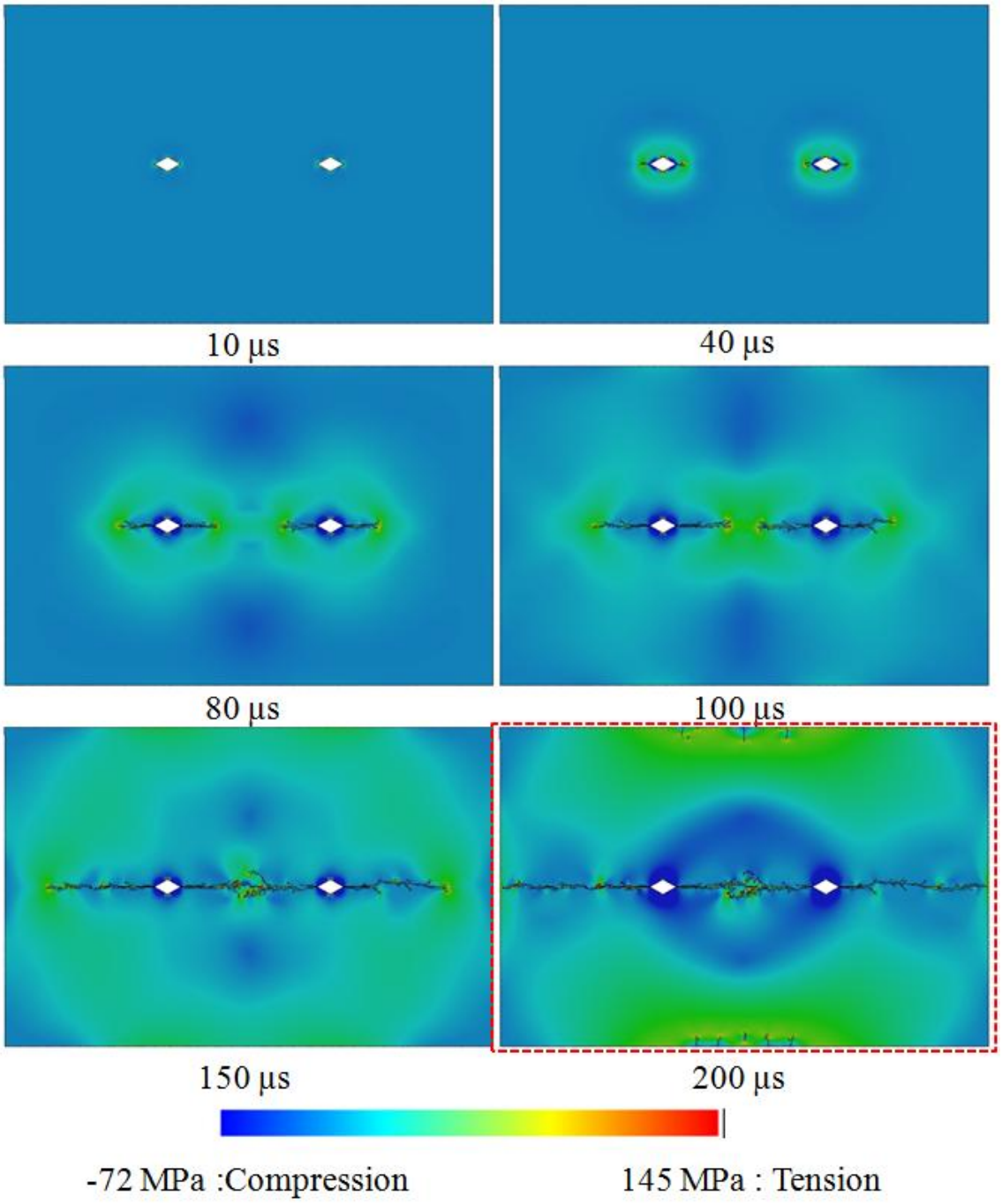

Figure 5.5 Result of fracture process in Case 3 (P_0=50 MPa, t_0=100 μs)

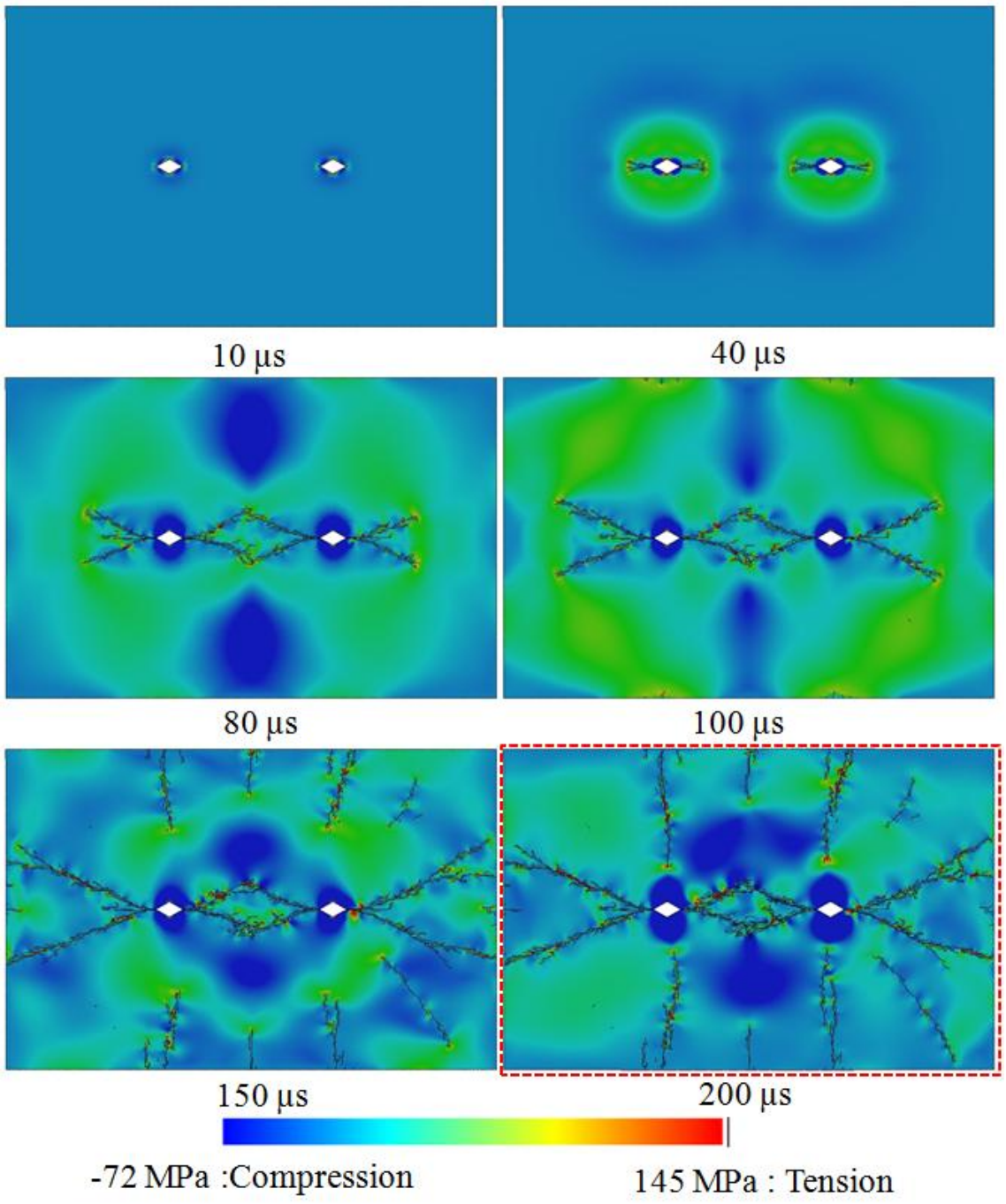

Figure 5.6 Result of fracture process in Case 5 (P_0=150 MPa, t_0=100 μs)

5.3.3 Comparison of resultant fracture patterns under various loading conditions

To examine the influence of the t_0 and P_0 on the resultant fracture pattern, the DFPAs corresponding to Cases 1 ~ 5 in Table 5.2 are conducted. Figure 5.7 shows the comparison of fracture patterns for each pressure conditions at t = 200 μs. For the resultant fracture patterns of Case 1 ~ 3 under various t_0 with fixed P_0, the smoothness of fracture plane in Case 1 became rougher than those in Cases 2 and 3. In addition, the crack initiation from upper and lower free faces is also found in Case 1 and this type of cracking is slightly and hardly observed in Cases 2 and 3, respectively. Therefore, if the t_0, i.e. loading rate becomes larger, the extension of cracking from outer free faces could be larger and thus the usage of explosive causing relatively smaller loading rate should be adopted.

On the other hand, for the resultant fracture patterns of Cases 2, 4 and 5 under various P_0 with fixed t_0, the results clearly show the degree of significant crack branching from each charge holder becomes more intense. Thus, an increase of P_0 can act as excessive energy supplier to the tip of initiated cracks and result in the branched cracking from the charge holders, i.e., unstable crack growths. Thus, the rougher fracture patterns are obtained with the increase of P_0. In addition, the increase of P_0 triggers the significant crack initiations from the outer free faces because the intensity of the induced stress level becomes higher resulting in the larger arc-like swelling perpendicular to the free face. From above comparison, it is clear that the P_0 should not exceed 50 MPa in order not to cause the major damage to the remaining part of concrete.

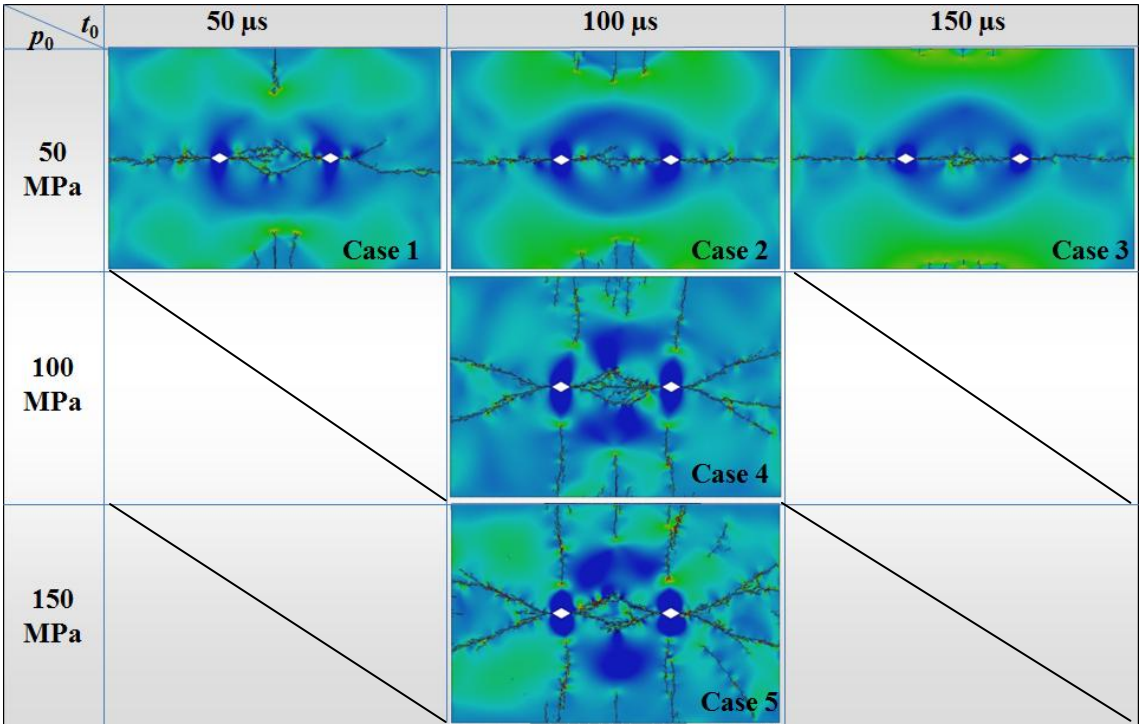

Figure 5.7 Comparison of resultant fracture patterns (t = 200 μs) for different pressure conditions

5.4 DISCUSSION

The above comparison with respect to the resultant fracture pattern under different loading conditions indicates that the occurrence of crack branching has quite important role in the fast fracturing processes (*e.g.*, Yoffe 1951; Knauss 1984; Ravi-Chandrar 1984; Meyers 1994; Ma *ea al*. 2005; Katzav *et al*. 2007). In the current problem, the main cause of crack branching can be owing to either interaction of stress waves from each charge holder or excessive supply of strain energy to the region in the close vicinity of crack tips. To investigate this in detail, by setting the monitoring line connecting to charge holders as shown in Fig. 5.8, the temporal change of the positions of crack tip with the largest distances from each charge holder are calculated by mapping the crack position onto the monitoring line. In addition, the temporal

profiles of compressive and tensile stress wave fronts from each charge holder along the monitoring line are calculated. Owing to the application of wedged charge holder, the detection of the compressive stress wave front entails a difficulty as shown in Fig. 5.9. Thus, the arrival time of compressive stress wave front is represented by the time calculated by the extrapolation from the maximum tangent of the compressive stress-time curve as shown in the figure. On the other hand, the arrival time of tensile stress wave front is simply calculated by finding the time when the compressive wave becomes zero.

Figure 5.9 shows the temporal profile of compressive, tensile stress wave fronts and the longest crack tips from each charge holder along the monitoring line shown by green, red and black lines, respectively. From the figure, it is found that the positions of the tips of longest tensile cracks from each charge holder closely follow the tensile wave front in call cases. It is also found that the arrival time of tensile stress wave front and, accordingly, the tips of the tensile crack becomes clearly shorter with the decrease of t_0 (See. Cases 1, 2 and 3) and increase of P_0 (See. Cases 2, 4 and 5). In addition, it is found from the result of Case 5 that the compressive stress wave fronts have not crossed with each other at $t = 40$ μs. Then, by referring to the result of $t = 40$ μs in Fig. 5.6 (Case 5) in which the crack branching has already occurred, it is now clear that the reason of the crack branching is not due to the stress interference in the central region but due to the excessive supply of strain energy to the region in the close vicinity of crack tips characterized by fast crack propagation. Based on this, the apparent of crack tip velocity for all the cases is calculated through the secant of temporal profile between the time intervals shown in Fig. 5.10.

In Table 5.3, the apparent of crack tip velocities for each case is shown. As is evident from this result, the crack velocity becomes clearly higher with the decrease of t_0 (See. Cases 1, 2 and 3) and increase of P_0 (See. Cases 2, 4 and 5). Compared to the S-wave velocity used in the DPFA which has a good correlation with Rayleigh wave velocity (Ravi-Chandar, 2004), the obtained apparent crack velocity of Case 3 with the result of almost straight crack only shows the smaller value of S-wave velocity while the other cases exceed the S-wave velocity and Case

5 with the most significant crack branching showed the highest crack tip velocity. Therefore, the pressure condition of Case 3 can be considered to cause the stable crack growth whereas those of the other cases, especially Cases 1, 4, and 5 can be considered to cause unstable crack growth condition. Therefore, for the achievement of well-controlled straight crack propagation using this method, the applied pressure should be carefully tuned to realize the stable crack growth condition and DFPA can be the powerful tool to investigate this optimum condition. Among the target pressure condition in this chapter, the condition of $t_0 \geq 150$ μs and $P_0 \leq 50$ MPa is suggested to cause stable crack growth.

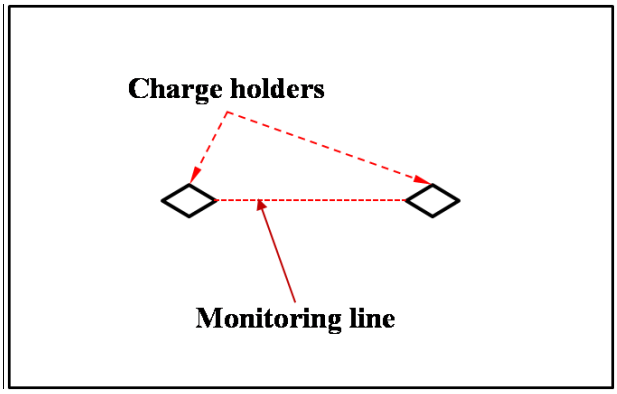

Figure 5.8 Monitoring line for stress wave fronts and crack tip position.

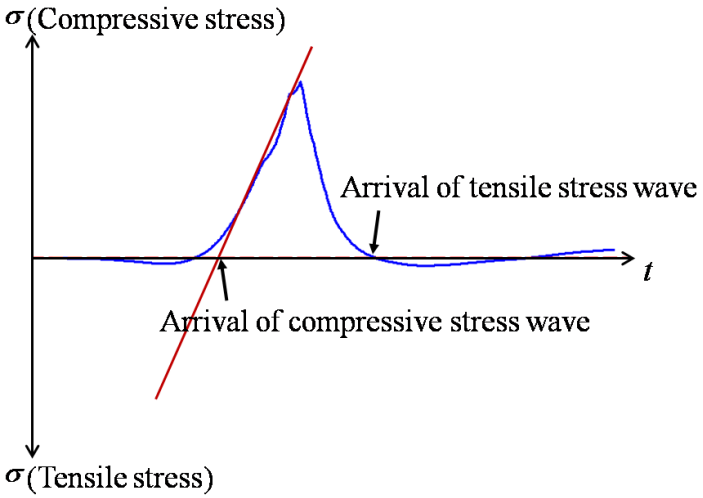

Figure 5.9 Calculation of arrival times of compressive and tensile stress wave fronts.

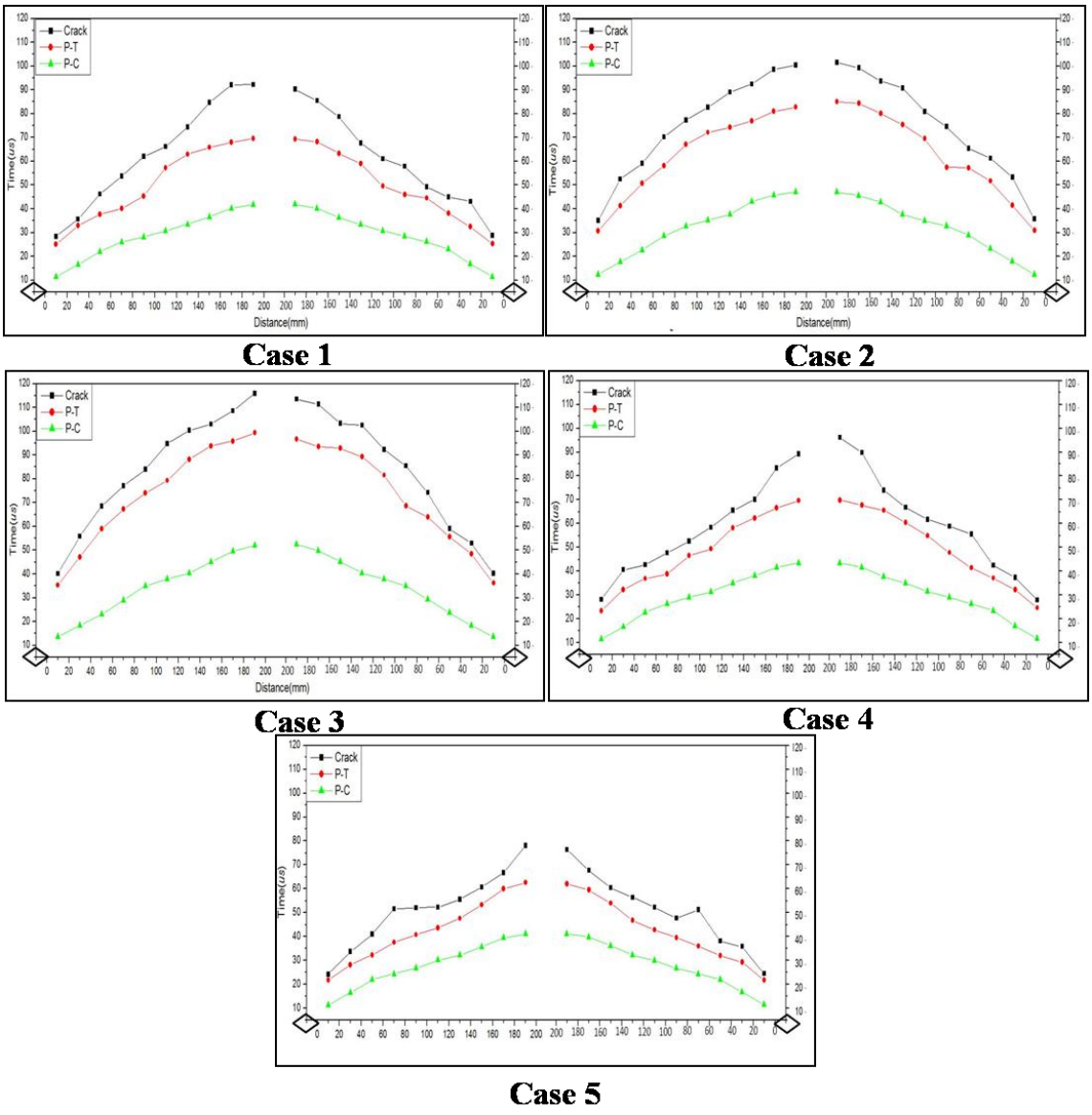

Figure 5.10 Temporal profile of positions of crack tip and compressive and tensile stress wave fronts along the monitoring line defined in Fig. 5.8.

Table 5.3 Comparison of average velocities of crack tips on crack.

Model	The average velocity of crack tip (km/s)
Case 1	2.8
Case 2	2.7
Case 3	2.3
Case 4	2.9
Case 5	3.3

5.5 CONCLUDING REMARKS

In this chapter, a dynamic breakage system through blasting with wedged charge holders by Nakamura et al. (2010) for the removal of a rectangular concrete structure was numerically investigated. To simulate the fracturing in huge concrete pile with rectangular cross section occurring over multiple charge holders, the DFPA for 2-D plane strain problem assuming the field-scale experiment of concrete structure by blasting with wedged charge holders was conducted in which the influence of maximum pressure P_0 and rise time t_0 of the applied pressure on the resultant fracture pattern was investigated.

From the comparison of parametric analysis of P_0 and t_0 by DFPA, it was clarified that the $t_0 \geq 150$ μs and $P_0 \leq 50$ MPa resulted in the best performance in which the well-controlled resultant fracture plane characterized by stable and almost straight crack propagation is obtained. It was also found that that more or less crack branching characterized by unstable crack growth occurred if the above condition was not satisfied and thus resulted in the non-controlled resultant fracture plane. In addition, through the calculation of the apparent crack velocity for each pressure condition, the crack branching was shown to be characterized by very fast crack propagation which was enhanced by higher P_0 and smaller t_0. Therefore, it is conclude that the care must be taken for the selection of the applied explosive to utilize the wedged charge and the realization of generated pressure to achieve the stable crack growth condition is necessary in which the DFPA can be the powerful tool to estimate this optimum condition.

BIBLIOGRAPHY

1) Cho, S.H., 2003, Dynamic fracture process analysis of rock and its application to fragmentation control in blasting, Doctor dissertation, Hokkaido University, Japan.

2) Cho, S.H., Ogata, Y. and Kaneko, K., 2003a, Strain rate dependency of the dynamic tensile strength of rock. Int. J. Rock. Mech. Min. Sci., Vol.40, No.5, pp. 763-777.

3) Cho, S.H., Nishi, M., Yamamoto, M. and Kaneko, K., 2003b, Fragment size distribution in blasting, Mater. Trans, Vol.44, No.5, pp.951-956.

4) Cho. S.H. and Kaneko, K., 2004, Influence of the applied pressure wave form on the dynamic fracture processes in rock, Int. J. Rock Mech.Min. Sci., Vol. 41, pp.771-784.

5) Cho, S.H., Mohanty. B., Ito, M., Nakamiya, Y., Owada, S., Kubota, S., Ogata, Y., Tsubayama, A., Yokota, M. and Kaneko, K., 2006, Dynamic fragmentation of rock by high-voltage pulses, Int. Proceedings of 41st US symposium on rock mechanics, Curran Associates, Inc., 06-1118.

6) Cho, S.H., Nakamura, Y., Mohanty. B, Yang. H.S, Kaneko. K, 2008, Numerical study of fracture plane control in laboratory-scale blasting, Engineering Fracture mechanics, Vol. 75(13), pp.3966-3984.

7) Fukuda, D., Moriya, K., Kaneko, K., Sasaki, K., Sakamoto. R, Hidani. K, 2012, Numerical simulation of the fracture process in concrete resulting from deflagration phenomena, Int. J. Fract, Vol. 180(2), pp. 163-175.

8) Ma, L, Wu, L and Guo, L.C, 2005, On the moving Griffith crack in a nonhomogeneous orthotropic strip, International Journal of Fracture, Vol.136, pp.187-205.

9) Meyers, M.A., 1994, Dynamic Behavior of Materials, John Wiley and Sons, Inc, pp.488-566.

10) Nakamura. Y, Kato. M, Ogata. Y, Okina. Y, Nakamura. S, Yamamoto. M, 2009, Model experiments on fracture plane control in blasting, Japan Explosive Society, pp. 9-12 (In Japanese)

11) Nakamura, Y., Kato, M., Ogata, Y., Yamaura, I., Nakamura, S. and Cho, S.H., 2010, Dynamic fragmentation method using simple-type charge holder for fracture control in blasting, 10th conference on Japan Society of civil engineers, pp.117-120 [In Japanese].

12) Stark, A., 2010, Seismic methods & applications: A guide for the detection of geologic structures, Earthquake zones and hazards, resources exploration and geotechnical engineering, BrownWalker Press.

CHAPTER 6

CONCLUSIONS

This dissertation investigated the dynamic fracturing method for the breakage of concrete pile head by blasting. The contents and findings of this dissertation are summarized as follows:

Chapter 2 proposed Dynamic Fracture Process Analysis (DFPA) for 2-dimensional plane strain problem was reviewed and Dynamic Fracture Process Analysis for axisymmetric problem (DFPA-A) was formulated for the simulation of breakage of concrete pile. In DFPA-A, two kinds of tensile fracture, i.e., the tensile fractures within *r-z* plane and normal to *r-z* plane in the cylindrical coordinate (r, z, θ), are taken into account. In the modeling of the tensile fracture within *r-z* plane, inter cracking method is used to simulate crack initiation, propagation and coalescence and the cohesive law was adopted to simulate the nonlinear crack opening behavior due to the existence of fracture process zone near the crack tip. In the modeling of the tensile fracture normal to *r-z* plane, the stress-strain relation in each element was used to express the decohesion of crack surface. A concept of Crack Opening Strain (COS) was proposed for the modeling of cohesive law where COS wass defined as the ratio of the Crack Opening Displacement (COD) to arch length of subdomain which included one predominant crack. Contrary to the DFPA for 2-D plane strain problem, the DFPA-A was newly proposed method in this dissertation and thus, the DFPA-A code must be developed and its implementation and applicability were discussed in Chapter 3. Then, the DFPA-A was applied to the simulation of breakage of cylindrical concrete pile head in Chapter 4.

Chapters 3 examined that the DFPA-A code was developed and its implementation and applicability were investigated. In the DFPA-A, the conical crack pattern formed from the bottom of charge hole as well as predominant cracks radially extending from the charge hole were successfully simulated, which agreed with generally obtained fracture pattern from

dynamic splitting experiment. Additionally, the DFPA-A gives harmonic fracture patterns compared to those obtained by using DFPA for plane strain problem, which shows the validity of the proposed DFPA-A. By applying the DFPA-A to the fracturing simulation assuming a concrete pile by blasting a cylindrical charge, it was pointed out that the initiation and propagation of the oblique tensile fracturing, i.e. conical cracks, from the bottom corner of charge hole is inevitable.

Chapter 4 conducted for the controlling of the conical cracks from the bottom of charge hole, the laboratory scale experiment and numerical analysis of the dynamic fracturing in cylindrical concrete pile with hollow steel plate as a crack arrester were performed. The influences of both the loading rate characterized by rise time t_0 of the applied pressure and spacing between steel plate and charge hole, S_b, on the resultant fracture pattern and optima condition in terms of the minimization of the damage in the remaining part of the cylindrical concrete pile owing to the dynamic removal of concrete pile head were clarified.

In case that the rise time,t_0, was considered as variable, blasting conditions with the larger t_0 than 50 μs was found to be more effective for arresting the conical crack propagation and prevention of the damages in the remaining part of concrete pile below the steel plate. In addition, it was indicated that the larger t_0 could result in less r-θ tensile fractures below the steel plate. On the other hand, in case that the distance between charge hole and steel plate, S_b, was considered as variable, blasting conditions with the installation distance of the hollow steel plate less than 5 mm from charge hole was found to be more effective for arresting the conical crack propagation to the remaining part of concrete pile below the steel plate. Therefore, considering all the DFPA-A results, the application of loading condition which realizes the relatively slower loading rate, i.e. $t_0 > 50$ μs, and $S_b < 5$ mm should be used to obtain the optimized fracture pattern.

Chapter 5 for dynamic breakage system through with wedged charge holders, DFPA for 2-dimensional plane strain condition was simulated in huge concrete pile with rectangular cross

section and conducted in which the influence of loading conditions, P_0 and t_0 on the resultant fracture patterns was investigated.

By analyzing numerical results by DFPA for 2-D plane strain problem, it was verified that the $t_0 \geq 150$ μs and $P_0 \leq 50$ MPa resulted in the best performance in which the well-controlled resultant fracture plane characterized by stable and almost straight crack propagation is obtained.

To investigate monitoring line connecting to charge holders, the temporal change of the positions of crack tip with the largest distances from each charge holder are calculated by mapping the crack position onto the monitoring line. In addition, the temporal profiles of compressive and tensile stress wave fronts from each charge holder along the monitoring line were calculated. Through the calculation of the apparent crack velocity for each pressure condition, the crack branching was shown to be characterized by very fast crack propagation which was enhanced by higher P_0 and smaller t_0. Therefore, it was conclude that the care must be taken for the selection of the applied explosive to utilize the wedged charge and the realization of generated pressure to achieve the stable crack growth condition was necessary in which the DFPA could be the powerful tool to estimate this optimum condition.